

Half-metallicity versus Symmetry in Pt, Ni and Co-based Half Heusler Alloys: A First-principles Calculation

Madhusmita Baral^{1,2} and Aparna Chakrabarti^{2,3}

¹ *Synchrotrons Utilization Section, Raja Ramanna Centre for Advanced Technology, Indore - 452013, India*

² *Homi Bhabha National Institute, Training School Complex, Anushakti Nagar, Mumbai-400094, India and*

³ *Theory and Simulations Laboratory, HRDS, Raja Ramanna Centre for Advanced Technology, Indore - 452013, India*

Using first principles calculations based on density functional theory, we study the geometric, electronic, and magnetic properties of Pt, Ni and Co-based half Heusler alloys, namely, Pt BC , Ni BC and Co BC ($B = \text{Cr, Mn and Fe}$; $C = \text{Al, Si, P, S, Ga, Ge, As, Se, In, Sn, Sb and Te}$). We calculate the formation energy of these alloys in various crystal symmetries, which include, the (face-centered) cubic $C1_b$ ($F43m$), orthorhombic ($Pnma$), as well as hexagonal ($P62m$ and $P63/mmc$) structures. It has been observed that out of all the 108 structures, studied here, energetically stable cubic structure is observed for only 18 materials. These alloys are primarily having either a C atom or an A atom with a high atomic number. We also observe that along with the alloys with C atoms from group IIIA, IVA and VA – alloys with C atoms from group VIA are also found to be, by and large, energetically stable. To examine the relative stabilities of different symmetries in order to search for the respective lowest energy state for each of the above-mentioned systems, as well as to find whether a material in the ground state is half-metallic or not, we analyze the formation energy, and the electronic density of states, in detail. Based on these analyses, the possibility of existence of any *one-to-one relationship* between the *cubic symmetry* and the *half-metallicity* in these half Heusler alloys is probed. Subsequently, we predict about the existence of a few new *non-cubic* half Heusler alloys with substantially low density of states at one of the spin channels and reasonably *high spin polarization at the Fermi level*.

PACS numbers: 71.20.Be, 71.15.Nc, 71.15.Mb, 75.50.Cc

I. INTRODUCTION

The prediction and development of new half-metallic ferromagnets are of immense interest due to their potential for technological application.¹ The half-metallic (HM) ferromagnets (FM) are a type of FM material where spin polarization at the Fermi level (E_F) is high (expected to be 100%) which may have an application in the field of spintronics. Ever since the half-metallicity has been predicted, in half Heusler alloys (HHA), namely, NiMnSb and related isoelectronic compounds, PtMnSb and PdMnSb, on the basis of band structure calculations,² the field of half-metallic half Heusler alloys (HM HHA) has attracted the interest of the researchers.³ Here we wish to point out that, further on, we refer to all the materials with high (about 65 to 70%) to 100% spin polarization, as HM-like materials.

Many HM-like materials have been found theoretically, among the half and full Heusler alloys.^{2,4,5} The Curie temperature (T_C) of quite a few of these alloys is calculated to be higher than the room temperature which is essential for their application as an efficient and useful spin-injector material.⁶ For this application, the interest is indeed in magnetic HHAs. It has been seen that a large amount of work on NiMnSb and substitution at its different atomic sites has been carried out, both theoretically and experimentally.^{2,7} In order to search for new half-metals, a large number of general ABC type HHAs have also been studied in the literature, where A and B are transition metal atoms and C is an sp element.⁸

In the literature, most of the HHAs studied theoretically have been shown to possess half-metallic property in the cubic $C1_b$ phase with $F43m$ space-group.² However, only some of these have been experimentally synthesized.⁹ On the contrary, it has been seen in the literature that many of the half Heusler alloy samples exhibit non-cubic symmetries but there is no explicit discussion on the half-metallicity in these materials.¹⁰⁻²⁴ It has been observed that NiMnSb and some other $ABSb$, as well as $ABSn$ materials possess cubic $C1_b$ symmetry.²⁴ On the other hand, while NiMnGe is seen to exhibit an orthorhombic $Pnma$ space-group at room temperature,²⁵ NiMnGa has a hexagonal symmetric structure.²⁰ Further, $ABSi$ or $ABGe$ or ABP or $ABAs$ compounds are seen to exhibit either an orthorhombic structure (with $Pnma$ space-group) or a hexagonal phase (with either $P63/mmc$ or $P62m$ space-group).¹⁰⁻²³ In the literature, there are also reports that, many samples of HHAs are seen to exhibit more than one symmetries. For example, each of NiMnAs and NiMnP are reported to possess both orthorhombic and hexagonal structures.¹¹ Further, in the literature, it has been found that some materials, including CoMnSb^{26,27} and PtMnAl²⁸, exhibit site disorder, which is often associated with a larger effective unit cell. As for the magnetic properties, many of the HHAs studied in the literature are seen to be FM in nature, and it is observed that with the change in A and B elements, the magnetic property of the alloys changes as well.²⁹

In the literature, a large number of full Heusler alloys (FHA) as well as HHAs, has been studied which shows half-metallic-like behavior but, to the best of our knowledge, only those alloys are seen to have a *half-metallic-like* character which possess a *cubic* structure. Therefore, in this work, we aim to search and screen magnetic half-metals based on half Heusler alloys: our specific interest is to probe that whether the cubic symmetry is a *necessary but NOT sufficient condition for the half-metallicity* in the HHA materials. It is to be further noted that, full Heusler alloys are much more extensively studied, compared to the HHAs, but none of these FHAs is seen to exhibit a structure with hexagonal symmetry. On the contrary, it is seen that many HHAs exist in different crystal symmetries, which include, hexagonal structures (with space-groups $P\bar{6}2m$ and $P6_3/mmc$) as well as (face-centered) cubic $C1_b$ ($F\bar{4}3m$ space-group) and orthorhombic structures (with space-group $Pnma$). For example, while NiMnSb is a well-known cubic HHA, the change in C atom from Sb to As leads to an orthorhombic structure in the lowest energy state. There are other similar examples among the HHAs. Since many Ni-based HHAs are known to exist in phases other than the well-known cubic $C1_b$ phase, we aim to study the reason as to why there is this difference in stability in case of various symmetries in HHAs and if there is any systematics involved. Further, in forming A_2BC or ABC Heusler alloys, C atom from the p-block elements, of group IIIA, IVA and VA, are well-known in the literature. Here we probe whether C atoms from group VIA are also favored in forming stable Heusler alloys.

To this end, we choose three sets of compounds, namely, $CoBC$, $NiBC$ and $PtBC$. Choice of A atom is primarily driven by the existing work in the literature, which are based mainly on Ni and also some Co and Pt-derived HHA materials. Further, the B atom is chosen to be an element with high atomic magnetic moment keeping the spin-injection properties in mind. It is to be noted that we are interested in those alloys, which show both magnetism as well as half-metallicity. We study various materials in different possible space-groups to find and understand the symmetry of the phase with lowest energy for each of these materials. For this purpose, we analyze the formation energy; also partial and total density of states (DOS) in order to understand the extent of hybridization between different atoms of the alloys. Further, we try to understand the trend in similarities and differences in the magnetic and electronic properties of these three sets of materials. We specifically analyze the possibility of existence of a half-metallic-like property in these compounds in their lowest energy phases and probe if there is any *one-to-one relationship* between the *cubic symmetry* and the *half-metallicity* in the alloys, studied in this work. Consequently, we predict the possibility of a few new half-Heusler alloys exhibiting high *spin polarization at the Fermi level* (termed as SP henceforth) with or without having the cubic symmetry. In the next section, we discuss the methods of calculations, which are based on density functional theory. In the section followed by methodology, we present our results and discussion on the same. Finally, we summarize and conclude in the last section.

II. METHOD

First, we discuss in detail the space-groups we have considered in our present work. We probe four different crystal symmetries, which have been reported for various half-Heusler alloys so far, namely, cubic $C1_b$ (space-group $F\bar{4}3m$, no. 216), orthorhombic (space-group $Pnma$, no. 62), as well as hexagonal structures (space-group $P\bar{6}2m$, no. 189 and $P6_3/mmc$, no. 194). We have not carried out any calculations on any disordered structure in this paper due to the lack of any systematic input of structural data for the materials, studied here. In this paper, we have carried out calculations on Co, Ni and Pt-based systems; Co, Ni and Pt are taken as A atom. Cr, Mn and Fe have been considered as the B atom since we are interested in magnetic alloys and these B atoms are known to have high atomic moments. Further, for C atom, we have taken the following elements, Al, Si, P, S, Ga, Ge, As, Se, In, Sn, Sb and Te. In total, we have studied 108 different HHAs. We probe the symmetry of an alloy which has the lowest formation energy. Further, we have carried out in depth calculations of the electronic and magnetic properties of the energetically stable alloys. The half-Heusler alloys assume an ordered ABC structure, where the A and B atoms are elements with d-electrons, typically transition metal (TM) atoms and C atoms are elements with s,p electrons (termed as sp element).

In the lowest energy state, the most well-studied HHA **NiMnSb** has a $C1_b$ structure that consists of four interpenetrating face-centered-cubic (fcc) lattices with origin at the fractional positions, (0.25, 0.25, 0.25), (0.75, 0.75, 0.75) (0.5, 0.5, 0.5), and (0.0, 0.0, 0.0). We label these sub-lattices as W , X , Y and Z , respectively. In $C1_b$ structure of NiMnSb, the Ni atoms occupy the W sub-lattice and the X sub-lattice remain empty. Further, Mn and Sb atoms occupy the Y and Z sub-lattices, respectively.

CoMnGe is a HHA which exhibits an orthorhombic structure with $Pnma$ symmetry. Atoms here occupy a Wyckoff position of 4c symmetry. While each of Co, Mn and Ge atoms has four equivalent atoms with fractional coordinates x and z as variables, the y coordinate for all the four atoms is 0.25. The symmetry equivalent fractional coordinates according to the 4c point-group symmetry are as follows: $x, 0.25, z$; $-x+0.5, 0.75, z+0.5$; $-x, 0.75, -z$; $x+0.5, 0.25, -z+0.5$.

NiMnGa assumes a hexagonal structure ($P6_3/mmc$ space-group) where Ni, Mn and Ga have two equivalent atoms each. Ni atom occupies sites with point-group symmetry of 2d (1/3, 2/3, 3/4 and 2/3, 1/3 and 1/4); Mn atom occupies sites with 2a symmetry (0,0,0 and 0,0,0.5); and Ga atoms are found at the sites with 2c symmetry (1/3, 2/3, 1/4 and

2/3,1/3,3/4).

NiFeAs is found in a hexagonal structure ($P\bar{6}2m$ space-group). Atom Ni occupies the site with 3f point-group symmetry ($x,0,0$; $0,x,0$; $-x,-x,0$); atom Fe has the preference for a site which has a 3g point-group symmetry with fractional coordinates as follows: $x,0,0.5$; $0,x,0.5$; $-x,-x,0.5$. Atom As occupies two different Wyckoff positions with 1b and 2c point-group symmetries with fractional coordinates, $(0,0,0)$ and $(1/3,2/3,0.5)$ and $(2/3,1/3,0.5)$, respectively.

The equilibrium lattice constants and fractional coordinates of all these alloys have been optimized by doing full geometry optimization using Vienna Ab Initio Simulation Package (VASP)³⁰ which has been used in combination with the projector augmented wave (PAW) method.³¹ We have interchanged the Wyckoff positions of the A and B atoms in case of $P6_3/mmc$ and $P\bar{6}2m$ space-groups as well as varied the variable fractional coordinates, x_A and x_B in case of the latter space-group to find the structure with the lowest formation energy. x and z have been varied for all the three atoms A , B and C in case of $Pnma$ symmetry to arrive at the structure which yields the lowest formation energy among all. We report in this paper the results for the fully optimized geometries of the materials for each of the four space-groups mentioned above.

For exchange-correlation functional, generalized gradient approximation (GGA) over the local density approximation (LDA) has been used.³² We use an optimum energy cutoff of 500 eV for the planewave basis-set. The final energies have been calculated with a k mesh for which the convergence has been tested. The energy and the force tolerance for our calculations were 10 μ eV and 10 meV/Å, respectively. The mixing or formation energies (E_{form}) have been calculated³⁰ for probing the energetic stability of a material, using the equation $E_{form} = E_{tot} - \sum_i c_i E_i$, where i denotes different types of atoms present in the unit cell of the material and E_i is the standard state (bulk) energy of the corresponding atom, i .³⁰ These energies have been then analyzed to establish the energetic stability of the alloys in different crystal symmetries. The optimized geometries of the systems are compared with the results obtained in the literature, wherever the results are available. The detailed converged structures (fractional coordinates and lattice constants) will be reported separately.³³

For in-depth understanding of the magnetic and electronic properties, we have carried out relativistic spin-polarized *all-electron* calculations for the optimized structures of all the systems. These calculations have been performed using full potential linearized augmented planewave (FP-LAPW) program³⁴ with the generalized gradient approximation (GGA) for the exchange correlation functional.³² For obtaining the electronic properties, the Brillouin zone (BZ) integration has been carried out using the tetrahedron method with Blöchl corrections.³⁴ An energy cut-off for the planewave expansion of about 14 Ry is typically used. The cut-off for charge density is $G_{max} = 14$. The number of k points for the self-consistent field cycles in the irreducible BZ is about 300, 600 and 2300 in case of cubic, hexagonal, and orthorhombic, respectively. The convergence criterion for the total energy E_{tot} is about 0.1 mRy per atom. The charge convergence is set to 0.0001.

III. RESULTS AND DISCUSSION

A. Analysis of Electronic Stability: Formation Energy

We study Co, Ni and Pt-based half Heusler alloys, namely, $CoBC$, $NiBC$ and $PtBC$ ($B = Cr, Mn$ and Fe ; $C = Al, Si, P, S, Ga, Ge, As, Se, In, Sn, Sb$ and Te). We calculate the formation energy of these alloys in different crystal symmetries, which include cubic $C1_b$ ($F43m$), orthorhombic ($Pnma$), as well as hexagonal ($P\bar{6}2m$ and $P6_3/mmc$) structures. As per the formation energy calculations, out of the total 108 alloys, which have been studied in this work, 25 compounds are found to be energetically unstable in any of the symmetries probed here (with close to zero or positive value of E_{form}). 35 materials have reasonably low absolute value of formation energy (below -50 kJ/mol per f.u.). Out of that, six compounds have too low a value of E_{form} (lower than -10 kJ/mol per f.u.). It is to be noted here that a negative value of the formation energy obtained from the calculations indicates that at zero temperature, the compound is more stable than the bulk counterparts of the constituent elements. With a low value of formation energy, the stability of the compound is expected to be less. It is observed that out of the 108 compounds the energetically unstable ones mostly have a C atom which has a large atomic number (Z), specifically for the Co and Ni-based alloys. Figure 1 depicts the optimized symmetry for each of the 83 energetically stable compounds, which is obtained on the basis of formation energy from our first-principles calculations. In this Figure, the symbols o , c , $h1$ and $h2$ signify $Pnma$, $F43m$, $P6_3/mmc$ and $P\bar{6}2m$ space-groups, respectively. From this figure, we observe that, for alloys having Co as the A atom, the lowest energy structure predominantly corresponds to the orthorhombic structure. Cubic symmetry is found to be the lowest energy state, primarily for cases, which have a high Z element (Se, Sb and Te) as C atom as well as Mn or Fe as B atom. It is to be noted that for low Z elements as C atom, the lowest energy phase is, without exception, either an orthorhombic structure or one of the hexagonal structures in all the three Co, Ni and Pt-based alloys. When A atom is Ni, and B atom is Mn, the alloys with a high atomic number element, namely, Se, Sb and Te as C atom has cubic structure as the lowest energy state. However, for other

Table 1. Formation energy and Lattice Parameter for CoBC, calculated for cubic, hexagonal and orthorhombic structures. GS_{expt} gives the experimentally observed symmetries.

Material	$E_{F\bar{4}3m}$	$E_{P6_3/mmc}$	$E_{P\bar{6}2m}$	E_{Pnma}	a	a, c	a, c	a, b, c	GS_{expt}
	(kJ/mol)	(kJ/mol)	(kJ/mol)	(kJ/mol)	(Å)	(Å)	(Å)	(Å)	
					$F\bar{4}3m$	$P6_3/mmc$	$P\bar{6}2m$	$Pnma$	
CoCrAl	8.85	-31.06	25.65	-41.50	5.47	4.18, 4.77	5.98, 3.75	4.90, 4.03, 7.34	—
CoCrGa	21.98	-6.48	18.46	-7.29	5.47	4.17, 4.84	6.81, 2.94	4.94, 4.05, 7.32	—
CoCrSi	-57.32	-88.95	-100.00	-103.25	5.38	4.00, 4.99	5.83, 3.60	5.75, 3.61, 6.73	$Pnma^{10}$
CoCrGe	-9.15	-23.89	-20.48	-23.76	5.49	4.10, 5.11	6.05, 3.68	5.73, 3.84, 7.06	$P6_3/mmc^{13}$
CoCrP	-77.89	-96.42	-160.98	-168.72	5.35	3.87, 5.17	5.71, 3.53	5.73, 3.52, 6.68	$Pnma^{11,12}$
CoCrAs	-28.34	-18.19	-49.69	-52.78	5.53	4.05, 5.28	6.08, 3.67	5.95, 3.71, 6.99	$P\bar{6}2m^{11,12}$
CoCrS	34.26	-22.08	-44.12	-47.54	5.46	3.63, 6.71	5.74, 3.57	5.92, 3.47, 6.73	—
CoMnAl	23.70	-65.94	-49.45	-75.45	5.46	4.12, 5.03	6.86, 2.81	5.05, 3.99, 7.31	—
CoMnGa	41.72	-41.65	-34.74	-43.76	5.47	4.12, 5.18	6.76, 2.98	5.7, 4.05, 7.24	—
CoMnSi	-58.02	-118.66	-123.67	-129.68	5.38	3.97, 5.00	5.97, 3.50	5.72, 3.66, 6.87	$Pnma^{10}$
CoMnGe	-14.32	-53.13	-55.51	-56.65	5.50	4.09, 5.13	6.22, 3.52	5.83, 3.78, 7.08	$Pnma^{14,15}$
									$P6_3/mmc^{14,15}$
CoMnP	-100.06	-104.32	-177.82	-187.28	5.36	3.87, 5.14	5.85, 3.45	5.89, 3.46, 6.68	$Pnma^{11,12,16}$
CoMnAs	-57.81	-31.45	-74.94	-78.84	5.54	4.05, 5.31	6.12, 3.59	6.31, 3.62, 6.97	$Pnma^{11,12,17}$
CoMnSb	-28.27	8.81	17.64	8.81	5.82	4.35, 5.43	6.41, 4.00	5.43, 3.35, 7.53	$F\bar{4}3m^{18}$
CoMnS	-1.42	-18.71	-55.40	-52.94	5.44	3.65, 6.82	5.79, 3.53	5.98, 3.54, 6.74	—
CoMnSe	-16.25	32.25	-4.35	-10.41	5.63	4.18, 5.45	6.20, 3.67	6.22, 3.80, 6.98	—
CoMnTe	-22.52	55.71	46.83	—	5.86	4.42, 5.49	6.48, 3.95	—	—
CoFeAl	12.34	-70.16	-54.54	-83.53	5.50	4.11, 4.92	6.87, 2.66	4.96, 3.95, 7.30	—
CoFeGa	31.36	-39.77	-30.97	-44.02	5.52	4.12, 4.97	6.89, 2.69	5.00, 3.96, 7.33	—
CoFeSi	-58.07	-104.96	-106.88	-111.96	5.38	3.95, 4.19	5.93, 3.42	5.60, 3.61, 6.79	$Pnma^{10}$
CoFeGe	-16.63	-33.41	-24.35	-34.15	5.50	4.08, 5.50	6.13, 3.48	5.00, 3.92, 7.31	$P6_3/mmc^{15}$
CoFeP	-74.40	-78.98	-158.53	-162.25	5.36	3.86, 5.02	5.72, 3.47	5.69, 3.52, 6.52	$Pnma^{11,12}$
CoFeAs	-35.39	-6.29	-43.08	-43.28	5.54	4.07, 5.13	5.99, 3.60	5.92, 3.67, 6.82	$P\bar{6}2m^{11}$
CoFeSb	-7.16	34.19	55.79	34.32	5.81	4.33, 5.28	6.37, 3.85	5.27, 4.29, 7.55	—
CoFeS	15.59	68.60	-24.59	-28.08	5.46	3.64, 5.79	5.74, 3.60	5.84, 3.64, 6.44	—
CoFeTe	-18.52	86.20	80.25	—	5.86	4.40, 5.26	6.32, 3.96	—	—

C elements, it is observed that the o , $h1$ and $h2$ symmetries are preferred. For Pt-based systems, the situation is the same as in case of Co and Ni case: the cubic phase with high Z elements, Se, Sn, Sb and Te as C atom, has the lowest energy. However, it is not the favored symmetry when the C atom is having low Z . Here we point out that there are two relevant databases in the literature, where symmetries of the lowest energy state of many of the materials studied here are listed. We compare the results from these two databases here. Since Ref.36 deals with only the cubic $F\bar{4}3m$ symmetry for the half Heusler alloys, and also does not deal with the Pt-based materials, we compare only the cubic symmetry cases. We see the matching for the cases with C atom with high atomic number Z , namely, Sn and Sb, which are expected to yield cubic ground state, is good (Figure 1). Open Quantum Materials Database (OQMD)³⁵ is a more detailed database and goes beyond the Heusler alloy compounds. Out of our 108 cases, 23 systems are not listed in this database. 65 materials have been listed there against the cubic symmetry (notably, except two, all the other Pt-based systems are listed to be having cubic ground state) and overall a reasonably good matching is observed between our results and the data from this database.

To understand the relative stability of various symmetries in different compounds, the formation energies of the energetically stable 83 HHAs are shown in Tables 1 to 3. From the formation energy values we find that, many of the 83 materials are likely to exist in more than one crystal symmetry since the formation energies of these different symmetries are within a few meV per formula unit (f.u.) of each other. In Tables 1, 2 and 3, we highlight (in bold) the entries corresponding to the lowest formation energy. The experimentally available structures are also presented in these tables against the respective compound. We find that the predicted symmetries with the lowest energy for different materials, by and large, match with the literature, except for a very few materials.

Results on Cubic case – From Figure 1, we observe that group VIA seems the most favorable atom for formation of the HHAs in the cubic symmetry with $C1_b$ structure (space-group $F\bar{4}3m$). It is further observed that for larger

Table 2. Formation energy and Total Magnetic Moment per formula unit for NiBC, calculated for cubic, hexagonal and orthorhombic structures. GS_{expt} gives experimentally observed symmetries.

Material	$E_{F\bar{4}3m}$	$E_{P6_3/mmc}$	$E_{P\bar{6}2m}$	E_{Pnma}	a	a, c	a, c	a, b, c	GS_{expt}
	(kJ/mol)	(kJ/mol)	(kJ/mol)	(kJ/mol)	(Å)	(Å)	(Å)	(Å)	
					$F\bar{4}3m$	$P6_3/mmc$	$P\bar{6}2m$	$Pnma$	
NiCrAl	31.05	-53.58	-11.08	-54.66	5.54	4.17, 5.01	6.03, 3.79	4.96, 4.13, 7.31	—
NiCrGa	42.03	-29.92	-1.91	-29.80	5.53	4.16, 5.08	6.16, 3.69	5.08, 4.16, 7.20	—
NiCrSi	-31.86	-98.04	-110.48	-107.06	5.44	3.98, 5.09	5.88, 3.62	5.75, 3.62, 6.89	$Pnma^{10}$
NiCrGe	1.73	-38.00	-41.95	-39.01	5.55	4.08, 5.28	6.07, 3.73	5.89, 3.77, 7.16	—
NiCrP	-45.42	-83.87	-149.98	-153.25	5.44	3.83, 5.47	5.89, 3.51	5.85, 3.53, 6.82	$Pnma^{11,12}$
NiCrAs	-18.77	-16.16	-63.09	-67.03	5.61	4.03, 5.49	6.21, 3.63	6.14, 3.68, 7.10	$P\bar{6}2m^{11,12}$
NiCrSb	-8.08	20.64	13.22	51.76	5.89	4.32, 5.65	6.56, 3.92	5.24, 4.35, 7.54	—
NiCrS	53.56	-2.16	-30.50	-21.01	5.57	3.70, 6.80	5.89, 3.59	5.46, 3.64, 6.92	—
NiMnAl	-9.60	-97.46	-55.52	-97.00	5.61	4.13, 5.13	6.03, 3.78	5.12, 4.05, 7.30	—
NiMnGa	1.73	-73.04	-46.11	-4.23	5.64	4.13, 5.18	6.28, 3.54	4.90, 3.99, 7.33	$P6_3/mmc^{20}$
NiMnSi	-70.17	-122.69	-134.95	-140.61	5.45	3.95, 4.13	5.98, 3.51	5.85, 3.56, 6.89	$Pnma^{10}$
NiMnGe	-41.31	-64.70	-71.22	-73.12	5.57	4.08, 5.26	6.18, 3.59	6.01, 3.67, 7.11	$Pnma^{14,21}$
NiMnSn	-21.01	-23.29	7.77	—	5.89	4.38, 5.47	6.38, 4.16	—	$P6_3/mmc^{14,21}$
NiMnP	-88.22	-94.71	-162.77	-162.51	5.46	3.73, 6.09	5.85, 3.46	5.86, 3.44, 6.76	—
NiMnAs	-66.86	-41.15	-73.01	-71.68	5.63	4.10, 5.48	6.17, 3.68	6.17, 3.77, 7.02	$Pnma^{11,12}$
NiMnSb	-58.71	-8.86	-1.33	-8.89	5.90	4.37, 5.56	6.47, 4.03	5.56, 4.37, 7.57	$P\bar{6}2m^{11,12}$
NiMnS	-13.46	-33.52	-45.29	-41.32	5.58	3.72, 6.98	5.95, 3.65	6.20, 3.60, 6.93	$F\bar{4}3m^7$
NiMnSe	-33.25	-1.52	-14.48	-21.23	5.77	3.96, 6.91	6.28, 3.82	6.58, 3.79, 7.72	—
NiMnTe	-30.35	31.85	77.43	—	6.01	4.49, 5.55	6.52, 4.12	—	—
NiFeAl	-19.81	-91.48	-69.46	-94.45	5.55	4.09, 5.00	6.95, 2.62	4.96, 3.88, 7.49	—
NiFeGa	-6.3	-57.89	-44.79	-12.21	5.56	4.11, 5.05	6.97, 2.65	4.94, 3.87, 7.38	—
NiFeSi	-34.59	-110.89	-119.66	-122.06	5.44	3.95, 4.95	5.92, 3.42	5.46, 3.63, 6.87	$Pnma^{10}$
NiFeGe	-8.06	-45.75	-40.97	-42.52	5.56	4.08, 5.10	6.12, 3.50	5.27, 3.85, 7.21	$P6_3/mmc^{24}$
NiFeP	-30.26	-64.64	-142.42	-139.56	5.41	3.90, 5.06	5.83, 3.36	5.59, 3.50, 6.71	$P\bar{6}2m^{11,12}$
NiFeAs	-5.65	-12.95	-39.64	-36.52	5.59	4.12, 5.14	6.03, 3.62	5.47, 3.70, 7.05	$P\bar{6}2m^{11,12}$
NiFeS	47.08	41.83	-9.06	-10.83	5.51	4.06, 5.11	5.84, 3.66	5.64, 3.50, 7.21	—

C atoms of other groups as well (for example, In, Sn, and Sb) the cubic phase is more stable compared to other symmetries. Among materials studied here, 68 compounds seem to have energetically stable cubic phase, ground state or not. Out of that maximum (30) is Pt-based compounds. From theoretical study, many of these cubic compounds are reported to show half-metallic-like character in the cubic $C1_b$ structure.³ However, only a few among these have been experimentally synthesized and found to possess cubic $C1_b$ structure.^{7,18,22,24}

Results on Hexagonal $P6_3/mmc$ symmetry – In total 69 compounds out of 108 have negative formation energy in the case of *hexagonal Ni_2In type* structure (with space-group $P6_3/mmc$). Compared to the Co atom, with Ni and Pt atoms at the A site, more number of alloys seems to be having negative formation energy. Experimentally, CoFeGe is reported to have hexagonal structure. However, from our calculations the lowest energy state of CoFeGe is found to be orthorhombic; but, the formation energy in the hexagonal ($P6_3/mmc$) is close to that of the orthorhombic structure (Table 1). CoMnSi, CoMnGe and NiMnSi compounds are reported to exist in both hexagonal ($P6_3/mmc$) and orthorhombic ($Pnma$) structure. Our present calculation shows that the lowest energy state structure of these compounds is orthorhombic.

Results on Hexagonal $P\bar{6}2m$ symmetry – From our calculations, 68 compounds are found to possess a negative formation energy for the *hexagonal* structure with a space-group of $P\bar{6}2m$. Out of these compounds quite a few are experimentally synthesized and are indeed found to have hexagonal $P\bar{6}2m$ structure.^{11,12,16} However, there are few small differences. For example, NiCrSi is experimentally observed to have an orthorhombic structure. But from our calculation the lowest energy state is found to be hexagonal $P\bar{6}2m$, though it is to be noted here that the formation energy of orthorhombic structure is very close to that of the hexagonal $P\bar{6}2m$ structure. The energy difference is

Table 3. Formation energy and Total Magnetic Moment per formula unit for PtBC, calculated for cubic and hexagonal structures. GS_{expt} gives experimentally observed symmetries.

Material	$E_{F\bar{4}3m}$	$E_{P6_3/mmc}$	$E_{P\bar{6}2m}$	E_{Pnma}	a	a, c	a, c	a, b, c	GS_{expt}
	(kJ/mol)	(kJ/mol)	(kJ/mol)	(kJ/mol)	(Å)	(Å)	(Å)	(Å)	
					$F\bar{4}3m$	$P6_3/mmc$	$P\bar{6}2m$	$Pnma$	
PtCrAl	-60.54	-146.51	-101.12	-111.22	5.85	4.34 , 5.50	6.61 , 3.70	5.07, 4.14, 7.91	-
PtCrGa	-22.20	-95.85	-63.42	-45.77	5.86	4.34, 5.59	6.70 , 3.66	5.16, 4.14, 7.20	-
PtCrIn	-0.83	-30.08	0.88	-30.06	6.29	4.61, 5.76	7.82, 2.99	5.77, 4.63, 7.96	-
PtCrSi	-60.52	-115.22	-122.29	-128.17	5.80	4.21, 5.46	6.35, 3.77	6.11, 3.88, 7.39	-
PtCrGe	-31.12	-62.25	-58.21	-63.81	5.92	4.30, 5.80	6.55, 3.83	6.17, 3.99, 7.65	-
PtCrSn	-36.02	-50.16	-8.03	-50.16	6.24	4.58, 5.87	6.95, 4.02	5.87, 4.58, 7.93	$P6_3/mmc^{22}$
PtCrP	-28.22	-66.39	-100.78	-102.87	5.84	3.98, 6.71	6.41, 3.66	6.34, 3.72, 7.27	-
PtCrAs	-27.42	-12.34	-41.32	-39.84	6.00	4.28, 6.19	6.75, 3.65	6.37, 3.90, 7.65	-
PtCrSb	-49.52	-8.73	-8.48	-8.65	6.22	4.60, 6.01	7.16, 3.74	6.01, 4.62, 7.93	-
PtCrTe	-9.81	47.41	40.00	40.11	6.33	4.63, 6.20	7.42, 3.69	6.07, 5.19, 7.41	-
PtMnAl	-117.70	-184.86	-160.06	-184.47	5.98	4.35, 5.41	7.29, 2.86	5.33, 4.16, 7.84	$P6_3/mmc^{24}$
PtMnGa	-83.55	-131.60	-119.18	-128.34	6.00	4.36, 5.54	7.34, 2.88	5.41, 4.16, 7.89	$P6_3/mmc^{24}$
PtMnIn	-54.71	-70.14	-44.17	-70.11	6.27	4.62, 5.71	7.79, 2.97	5.71, 4.64, 7.97	-
PtMnSi	-109.35	-136.27	-156.04	-159.28	5.82	4.21, 5.48	6.39, 3.65	6.23, 3.75, 7.34	-
PtMnGe	-85.23	-84.27	-88.04	-88.20	5.95	4.35, 5.60	6.61, 3.70	6.27, 3.90, 7.59	$P6_3/mmc^{23}$
PtMnSn	-96.61	-75.29	-37.87	-75.22	6.22	4.61, 5.71	6.85, 4.18	5.71, 4.63, 7.96	$F\bar{4}3m^{24}$
PtMnP	-75.50	-70.07	-110.29	-104.96	5.86	4.00, 6.78	6.17, 3.63	6.14, 3.56, 7.86	-
PtMnAs	-82.47	-37.07	-51.27	-54.10	6.02	4.41, 5.70	6.68, 3.81	6.36, 4.05, 7.58	-
PtMnSb	-106.05	-33.61	-18.61	-33.71	6.23	4.64, 5.79	6.95, 4.08	5.78, 4.67, 8.00	$F\bar{4}3m^{24}$
PtMnSe	-32.21	19.46	7.34	-	6.14	4.52, 5.73	7.21, 3.46	-	-
PtMnTe	-56.86	-	33.40	7.32	6.35	-	7.44, 3.71	5.90, 5.40, 7.40	-
PtFeAl	-111.81	-160.19	-133.87	-167.48	5.88	4.33, 5.24	7.22, 2.76	5.17, 4.05, 7.93	-
PtFeGa	-71.15	-96.88	-88.74	-44.87	5.90	4.35, 5.31	7.31, 2.78	5.24, 3.98, 7.82	-
PtFeIn	-23.01	-23.72	-3.53	-23.77	6.16	4.60, 5.52	7.75, 2.87	5.52, 4.63, 7.93	-
PtFeSi	-71.51	-23.72	-122.73	-126.21	5.89	4.60, 5.52	6.07, 3.72	5.82, 3.85, 7.27	-
PtFeGe	-44.45	-45.35	-46.14	-21.62	5.91	4.33, 5.40	6.30, 3.74	5.33, 3.95, 7.81	-
PtFeSn	-48.64	-31.42	-2.19	-32.25	6.16	4.58, 5.57	7.64, 2.99	5.57, 4.71, 7.73	$P6_3/mmc^{22}$
PtFeP	-9.32	-14.53	-104.74	-87.24	5.81	4.26, 5.24	6.05, 3.63	5.95, 3.57, 7.75	-
PtFeAs	-10.42	12.40	-25.70	25.12	5.97	4.42, 5.40	6.32, 3.71	5.46, 3.92, 7.98	-
PtFeSb	-26.60	13.09	17.47	8.64	6.18	4.62, 5.59	6.58, 4.03	5.58, 5.05, 7.45	-

3.42 kJ/mol (34.2 meV per f.u.) which is of the order of the thermal energy. Experimentally, NiMnGe is found to possess orthorhombic and hexagonal ($P6_3/mmc$) structures. But from our calculation, the obtained lowest energy state is the orthorhombic structure. We see from Table 2 that, the formation energies for the orthorhombic and the two hexagonal structures are reasonably close to each other. Similar is the case for CoFeAs. It is seen to have a hexagonal $P\bar{6}2m$ structure from literature. But from our calculations, it is observed that both the $Pnma$ and the hexagonal phase have very close value of E_{form} , and the former is slightly more stable than the other (Table 1).

Results on Orthorhombic phase – From our calculations the compounds, which are found to be in *orthorhombic, NiTiSn type* structure with space-group $Pnma$, are primarily Co-based compounds. In total 70 alloys have energetically stable $Pnma$ structure. It is worth-noting that for most of the NiMnC structures, with a C atom with a low Z value, the ground state is found to be energetically very close to the orthorhombic phase. The symmetry of compounds at the lowest energy state matches with the reports in the literature, barring a few exceptions. While CoCrAs, CoMnGe and NiCrAs are found to exhibit a hexagonal symmetry, our calculations yield an orthorhombic lowest energy state for these alloys. However, it is to be noted that from Table 1 and 2, we observe that the formation energies of both these structures are very close (difference being 3 to 5 kJ/mol per f.u.). Another exception is the case of CoMnAs. It is found to possess orthorhombic phase as ground state but from experiment it is found to have $P6_3/mmc$ space-group. The energy difference, however, in this case, is large between these two phases (Table 1). For many compounds it is found that, the orthorhombic phase has a formation energy which is very close (within 5 meV per f.u.) to the E_{form} of one of the hexagonal phases. Hence, from our detailed analysis of E_{form} values, it can be

Table 4. Geometry Analysis: d gives the bondlength in Å. Unit of density is Mg/m³. In 3rd column, "Y" signifies there is good matching with the ground state XRD pattern.

Material	Symmetry	XRD	density	$d(A-B)$	$d(A-C)$	$d(B-C)$
PtCrSn	$P6_3/mmc$	-	11.41	3.02	2.64, 2.94	3.02
	$Pnma$	Y	11.41	3.02, 3.02, 3.03, 3.03	2.64, 2.64, 2.94, 2.94	3.02, 3.02, 3.02, 3.03
	$F\bar{4}3m$	N	10.01	2.70	2.70	3.12
	$P\bar{6}2m$	N	10.83	3.03, 3.24	2.63, 2.68	2.90, 2.90, 2.91
PtMnIn	$P6_3/mmc$	-	11.48	3.03	2.67, 2.86	3.03
	$Pnma$	Y	11.48	3.00, 3.00, 3.04, 3.04	2.67, 2.67, 2.86, 2.86	3.02, 3.03, 3.03, 3.03
	$F\bar{4}3m$	N	9.81	2.72	2.72	3.14
	$P\bar{6}2m$	N	11.66	2.97, 3.02	2.71, 2.80	2.83, 2.89, 2.89
PtFeIn	$Pnma$	-	12.00	2.96, 2.96, 3.01, 3.01	2.66, 2.66, 2.76, 2.76	2.99, 2.99, 2.99, 3.00
	$P6_3/mmc$	Y	12.00	2.99	2.66, 2.76	2.99
	$F\bar{4}3m$	N	10.39	2.67	2.67	3.08
	$P\bar{6}2m$	N	12.21	2.95, 2.98	2.69, 2.78	2.79, 2.87, 2.87
PtMnSn	$F\bar{4}3m$	-	10.17	2.69	2.69	3.11
	$P6_3/mmc$	N	11.65	3.02	2.66, 2.86	3.02
	$Pnma$	N	11.65	3.00, 3.00, 3.03, 3.03	2.66, 2.66, 2.86, 2.86	3.02, 3.02, 3.02, 3.02
	$P\bar{6}2m$	N	10.80	2.87	2.62, 2.70	2.89, 3.18
PtMnSb	$F\bar{4}3m$	-	10.20	2.70	2.70	3.12
	$Pnma$	N	11.44	3.02, 3.02, 3.06, 3.06	2.68, 2.68, 2.89, 2.89	3.04, 3.04, 3.05, 3.05
	$P6_3/mmc$	N	11.44	3.05	2.68, 2.90	3.05
	$P\bar{6}2m$	N	10.87	3.04	2.61, 2.72	2.90, 2.92, 2.92
NiMnAs	$P\bar{6}2m$	-	7.75	2.77, 2.88	2.35, 2.41	2.55, 2.62
	$Pnma$	N	7.67	2.75, 2.85, 2.90, 2.91	2.34, 2.36, 2.42, 2.69	2.56, 2.60, 2.69
	$F\bar{4}3m$	N	7.00	2.44	2.44	2.82
	$P6_3/mmc$	N	7.84	2.74	2.37, 2.74	2.74
NiMnAl	$P6_3/mmc$	-	6.16	2.71	2.39, 2.57	2.71
	$Pnma$	N	6.18	2.53, 2.64, 2.78, 2.93	2.41, 2.44, 2.54, 2.58	2.63, 2.64, 2.72, 2.95
	$P\bar{6}2m$	N				
	$F\bar{4}3m$	N	5.26	2.43	2.43	2.81
CoCrGe	$P6_3/mmc$	-	8.20	2.69	2.37, 2.55	2.69
	$Pnma$	N	7.85	2.65, 2.77, 2.79, 2.81	2.33, 2.36, 2.37	2.58, 2.59, 2.63
	$P\bar{6}2m$	N	7.87	2.71, 2.90	2.33, 2.36	2.57, 2.58
	$F\bar{4}3m$	N	7.37	2.38	2.38	2.75

inferred that the orthorhombic structure is the most common symmetry among the Co-based materials. There are quite a few of the Ni and Pt-based materials for which also this structure has the lowest energy. As discussed above, in many cases two or more phases are close in energy. Hence, it is likely that samples of the non-ground state phases of these materials may actually form under certain experimental conditions.

B. Geometry Analysis: Lowest Energy State versus Other States

The lattice parameters for all the energetically stable materials are given in Tables 1 to 3. The cubic phase has a relatively open structure. Hence, a cubic phase is found to be the lowest energy state for materials with atoms with larger atomic radii and larger Z values (of Pt and some of the C atoms).

There are about twelve systems where the E_{form} values of two phases are very close and these values are within 1 kJ/mol per f.u. To understand this small difference in the E_{form} , we perform a detailed geometry analysis. Table 4 gives relevant data for some typical materials, where in a few cases there is an excellent matching of the E_{form} between two symmetries and where there is no matching. In this table, along with the density values and the bondlength between two atoms (d), we have also noted if the simulated X-ray diffraction (XRD) pattern³⁰ of the phase matches with the same of the ground state structure or not. We present the data of all the symmetries for each material

where first, second, third and fourth rows correspond to the ground state (GS) and the three other phases, having difference in formation energy with the ground state in an increasing order: these are described as $GS+1$, $GS+2$ and $GS+3$ states. For PtCrSn and PtMnIn it is observed from Table 3 that, $P6_3/mmc$ is the ground state. However, it is seen that the respective $Pnma$ phases, that is the $GS+1$ phase in these two systems, possess a E_{form} energy which is very close to the ground state (within 0.01 kJ/mol/f.u.). Similarly, PtFeIn has a $Pnma$ structure as the lowest energy state and $P6_3/mmc$ structure also has a very similar value for the formation energy (Table 3). From Table 4 it is clear that the XRD patterns of these two symmetries for the three above-mentioned materials are expected to be close. Additionally, the densities of these two phases for PtCrSn, PtMnIn and PtFeIn are close to each other. When we compare the bondlength d between the atoms $A-B$, $A-C$ and $B-C$ for the two symmetries for these three materials, we note that the values vary maximum by only ± 0.03 Å. Since the density, bondlengths and the simulated XRD patterns match so well, it is clear that the internal local geometries of each atom and subsequently the bonding nature in the two phases with two different symmetries for each of these three materials are the same. It is also clear from Tables 1 to 4 that the other two symmetries ($F43m$ and $P62m$) are not only energetically farther from the ground state, but these are also different from the geometric point of view. In case of NiCrGa (Table 2), and PtCrIn (Table 3) also similar results are obtained. While these two symmetries ($P6_3/mmc$ and $Pnma$) in NiCrGa show good overall matching, in case of PtCrIn, the XRD patterns are found to be not quite close.

Further, it is interesting to probe PtMnSn and PtMnSb for the following reason. It is observed that the ground state symmetry is cubic in both the cases. When the data for these two materials from Table 4 are analyzed it is found that, while the geometric data of the ground state symmetry does not match with those of any of the other three symmetries, all the data from second and third row (for phases $Pnma$ and $P6_3/mmc$) match very well. Table 3 lists the respective formation energies for these two materials and we observe that these data are indeed consistent with this observation. Subsequently, the XRD patterns of these materials for the two above-mentioned symmetries are seen to resemble each other. Next we discuss a few cases, where the E_{form} value of one symmetry is only somewhat close to the ground state. We take the example of NiMnAs. The ground state $P62m$ has a E_{form} (-73.01 kJ/mol per f.u.) and density values (7.75 Mg/m³); the $Pnma$ symmetry has somewhat close values for these two quantities (-71.68 kJ/mol per f.u. and 7.67 Mg/m³, respectively). Consequently, the geometric data including simulated XRD patterns of the two phases also exhibit not a good matching with each other. Similar is the case for materials, for example, NiMnAl, CoCrGe, PtMnAl and PtMnGe.

C. Analysis of Total and Partial Moment

In this subsection, we discuss the results on the magnetic properties of the materials, studied here. The calculations are carried out with a magnetic configuration for all the materials. Since Co has a significant moment, there is a possibility that a ferrimagnetic (moments of Co and B atom aligned anti-parallel to each other) configuration may be likely. After convergence we get, in a few cases a ferrimagnetic and in most of the cases a FM configuration as observed in the literature.^{3,27} We present in Tables 5 to 7, the total, partial moments, the total number of valence electrons, and the SP of all the materials, wherever possible. The results of the cubic case and the lowest energy state obtained from our calculations are listed in these tables. When cubic is the symmetry for the lowest energy state, the explicit entries corresponding to the cubic case (on the left side of the Tables 5 to 7) are left empty. Values corresponding to energetically unstable cases have also been put (in italics) to see whether any trends which are found for the stable cases are followed by these or not.

Slater-Pauling rule, and Integer Moment versus Half-metallicity in Cubic case – It is observed in the literature that many Co-based Heusler alloys, specifically the half-metallic ones, follow the Slater-Pauling rule.^{5,37,38} As a consequence of this rule, an almost linear variation of the magnetic moment with the atomic number of the B atoms for the cubic case of the Co-based FHA materials is observed. In this work also we expect that a linearly increasing trend of the total moment as a function of the Z value of the C atom will be observed in the cubic cases of $CoBC$. Figure 2 shows the $CoMnC$ cases. The cases with positive E_{form} are also plotted for overall comparison. We find that the linear trend is not quite followed when the E_{form} of the compound is positive. However, the total moment of the energetically stable alloys shows this linear trend as is clear from both Figure 2 and Table 5. These findings are true for $CoCrC$ systems as well. We further observe from Figure 2 that though like the total moment, the partial moments, mainly that of B atom also show an increasing trend, there is a change of slope in both the cases of the A and B atoms, as is true for stable $CoCrC$ systems also. It is to be noted that none of these trends are followed in case of $CoFeC$. Figure 2 exhibits a few Ni and all Pt-based cases as well. In case of Ni and Pt-based systems, in general, none of these above-mentioned trends is observed. The moments of the $NiFeC$ alloys are seen to all together deviate from the trend. On the contrary, $NiCrC$ and $NiMnC$ cases with C atoms from group IVA, VA and VIA tend to follow the Slater-Pauling rule, when the E_{form} is negative and C atom has a lower atomic number. As the group of the C atoms changes, from IVA to VA to VIA, the total moment increases (by value 1), and partial

Table 5. Total and Partial Magnetic Moment per formula unit (in units of μ_B) for CoBC, calculated for cubic phase (*CS*) and the lowest energy structure (*GS*). The numbers are put in italics when the corresponding formation energy is positive. NVE is the number of valence electrons, *SP* is the spin polarization at the Fermi level.

Material	NVE	<i>CS</i>					<i>GS</i>				
		μ_T	μ_A	μ_B	μ_C	<i>SP</i>	μ_T	μ_A	μ_B	μ_C	<i>SP</i>
CoCrAl	18	<i>0.00</i>	<i>0.00</i>	<i>0.00</i>	<i>0.00</i>	<i>0.43</i>	1.43 (Pnma)	0.37	1.02	-0.01	54.5
CoCrGa	18	<i>0.00</i>	<i>0.00</i>	<i>0.00</i>	<i>0.00</i>	<i>0.51</i>	1.57 (Pnma)	0.36	1.18	-0.02	52.4
CoCrSi	19	1.00	-0.17	1.17	-0.03	99.9	0.99 (Pnma)	-0.03	1.04	-0.02	
CoCrGe	19	1.00	-0.30	1.31	-0.05	100	2.40 (<i>P6₃/mmc</i>)	0.55	1.84	-0.05	7.03
CoCrP	20	2.00	-0.01	1.95	-0.05	100	1.93 (Pnma)	0.24	1.73	-0.04	76.3
CoCrAs	20	2.00	-0.25	2.19	-0.07	100	2.18 (Pnma)	-0.15	2.33	-0.07	52.2
CoCrS	21	<i>3.00</i>	<i>-0.17</i>	<i>2.81</i>	<i>0.02</i>	<i>97.9</i>	2.94 (Pnma)	0.29	2.61	-0.04	58.0
CoMnAl	19	<i>1.03</i>	<i>-0.20</i>	<i>1.36</i>	<i>-0.03</i>	<i>78.7</i>	3.32 (Pnma)	0.78	2.65	-0.04	18.4
CoMnGa	19	<i>3.00</i>	<i>0.37</i>	<i>2.69</i>	<i>-0.06</i>	<i>95.6</i>	4.12 (Pnma)	1.15	3.12	-0.09	34.7
CoMnSi	20	2.00	0.03	2.14	-0.06	100	3.49 (Pnma)	0.67	2.98	-0.06	41.2
CoMnGe	20	2.00	-0.19	2.36	-0.09	100	3.75 (Pnma)	0.71	3.22	-0.09	44.0
CoMnP	21	3.00	0.11	2.90	-0.06	100	2.99 (Pnma)	0.32	2.79	-0.05	13.8
CoMnAs	21	3.00	-0.06	3.08	-0.04	100	3.10 (Pnma)	0.12	3.09	-0.07	52.9
CoMnSb	21						3.00 (Cubic)	0.15	3.24	-0.08	100
CoMnS	22	4.00	0.42	3.37	0.03	100	2.39 (<i>P6₂m</i>)	-0.09	2.52	-0.06	13.8
CoMnSe	22						4.00 (Cubic)	0.37	3.47	0.00	97.8
CoMnTe	22						4.00 (Cubic)	0.38	3.56	-0.03	100
CoFeAl	20	<i>2.64</i>	<i>0.64</i>	<i>2.27</i>	<i>-0.05</i>	<i>58.7</i>	3.26 (Pnma)	1.03	2.41	-0.04	49.7
CoFeGa	20	<i>2.72</i>	<i>0.61</i>	<i>2.36</i>	<i>-0.08</i>	<i>21.4</i>	3.41 (Pnma)	1.04	2.52	-0.06	45.3
CoFeSi	21	3.00	0.65	2.52	-0.05	94.4	2.56 (Pnma)	0.56	2.18	-0.04	66.0
CoFeGe	21	3.00	0.51	2.71	-0.09	100	2.72 (Pnma)	0.62	2.25	-0.06	63.7
CoFeP	22	3.86	0.99	2.84	0.01	1.1	2.04 (Pnma)	0.36	1.80	-0.04	23.2
CoFeAs	22	3.98	1.04	2.93	0.0	66.1	2.14 (Pnma)	0.25	2.02	-0.04	45.9
CoFeSb	22						3.99 (Cubic)	1.04	2.99	-0.02	58.3
CoFeS	23	<i>4.94</i>	<i>1.55</i>	<i>3.13</i>	<i>0.19</i>	<i>18.7</i>	2.98 (Pnma)	0.62	2.39	0.03	33.6
CoFeTe	23						4.42 (Cubic)	1.25	3.07	0.07	69.5

moment of both Ni and *B* atoms increases. This observation has been discussed again in the next subsection in terms of the DOS of the up and down spin electrons. As the group of the *C* atom remains the same and the period changes, the total moment remains the same, but moment of Ni and *B* atoms decreases and increases, respectively. For the Pt-based systems, the Slater-Pauling rule of linear increase of total moments is not obeyed (Figure 2). Further, it has been observed that for the cubic cases, in many of the materials (maximum for the Co-based systems), the moment is integral in nature. It is expected that typically an integral moment leads to a half-metallic system in cubic phase. It will be discussed in detail in the next subsection after analyzing the total density of states of the up and down spin electrons, for both cubic and non-cubic systems.

Partial Moments in the Cubic case – Here we concentrate on the cubic phases of the materials. It is observed from the partial moments that for some of the cases the final configuration has turned out to be ferrimagnetic. In the literature, it has been discussed³ that there is a dependence of the long-range magnetic configuration on the number of valence electrons (NVE). While systems with NVE=18 (case **a**) show anti-ferromagnetism, cases with NVE=19 and 20 (case **b**) exhibit ferrimagnetism. On the contrary, NVE=21 and 22 (case **c**) lead to ferromagnetism. The *B* atom carries the maximum moment in all these cases discussed here. The moment on the *A* atom is almost equal in magnitude and opposite in direction in case **a**. In case **b**, moment on *A* is smaller in magnitude but oriented in an anti-parallel arrangement with respect to moment of *B* atom. On the contrary, case **c** deals with a long range FM configuration, where both *A* and *B* moments, though may be unequal, orient along the same direction. By analyzing our results (Tables 5, 6 and 7) on the partial moments of the energetically stable cubic phase, we find that there are only a few exceptions. While Co and Ni-based systems generally follow the trend, maximum deviation is observed in case of Pt-based systems. We have found that for NVE=23 also, the results follow the trend as in case **c**.

Total and Partial moments in the Ground states – Here we concentrate on the total and partial moments of the phases with the lowest energy. Few of the cases exhibit a close-to-integral total moment (CoMnP, CoFeP, CoFeS,

Table 6. Total and Partial Magnetic Moment per formula unit (in units of μ_B) for NiBC, calculated for cubic (*CS*) and the lowest energy structure (*GS*). The numbers are put in italics when the corresponding formation energy is positive. NVE is the number of valence electrons, *SP* is the spin polarization at the Fermi level.

Material	NVE	<i>CS</i>					<i>GS</i>				
		μ_T	μ_A	μ_B	μ_C	<i>SP</i>	μ_T	μ_A	μ_B	μ_C	<i>SP</i>
NiCrAl	19	<i>1.00</i>	<i>-0.03</i>	<i>1.13</i>	<i>-0.04</i>	100	2.17 (<i>Pnma</i>)	0.28	1.78	-0.01	2.8
NiCrGa	19	<i>1.00</i>	<i>-0.10</i>	<i>1.19</i>	<i>-0.06</i>	100	2.35 (<i>P6₃/mmc</i>)	0.28	2.00	-0.03	9.4
NiCrSi	20	2.00	0.11	1.93	-0.07	100	2.30 (<i>P$\bar{6}2m$</i>)	0.23	2.14	-0.06	4.4
NiCrGe	20	<i>2.00</i>	<i>0.02</i>	<i>2.05</i>	<i>-0.11</i>	100	2.79 (<i>P$\bar{6}2m$</i>)	0.18	2.66	-0.07	26.5
NiCrP	21	3.00	0.17	2.69	-0.08	100	2.62 (<i>Pnma</i>)	0.17	2.47	-0.06	46.7
NiCrAs	21	3.00	0.06	2.84	-0.11	100	2.99 (<i>Pnma</i>)	0.09	2.87	-0.09	69.6
NiCrSb	21						3.05 (Cubic)	0.01	2.99	-0.11	81.6
NiCrS	22	<i>3.99</i>	<i>0.26</i>	<i>3.30</i>	<i>0.01</i>	98	2.40 (<i>P$\bar{6}2m$</i>)	0.08	2.24	-0.06	5.6
NiMnAl	20	3.12	0.19	3.15	-0.07	76.8	3.20 (<i>P6₃/mmc</i>)	0.25	2.99	-0.04	47
NiMnGa	20	<i>3.32</i>	<i>0.16</i>	<i>3.33</i>	<i>-0.11</i>	56.6	3.26 (<i>P6₃/mmc</i>)	0.25	3.10	-0.07	38.5
NiMnSi	21	3.00	0.20	2.96	-0.08	100	2.83 (<i>Pnma</i>)	0.16	2.81	-0.06	57.1
NiMnGe	21	3.01	0.10	3.09	-0.13	66.3	2.98 (<i>Pnma</i>)	0.09	3.06	-0.10	43.3
NiMnSn	21	3.35	0.06	3.47	-0.12	1.3	3.49 (<i>P6₃/mmc</i>)	0.17	3.40	-0.07	35.2
NiMnP	22	4.00	0.38	3.51	-0.03	100	2.33 (<i>P$\bar{6}2m$</i>)	0.01	2.42	-0.08	48.4
NiMnAs	22	4.00	0.32	3.61	-0.05	100	3.44 (<i>P$\bar{6}2m$</i>)	0.09	3.41	-0.05	8.9
NiMnSb	22						4.00 (Cubic)	0.26	3.72	-0.06	100
NiMnS	23	4.99	0.65	3.92	0.16	88.8	3.60 (<i>P$\bar{6}2m$</i>)	0.20	3.32	0.00	21.8
NiMnSe	23						4.96 (Cubic)	0.60	4.00	0.13	78.3
NiMnTe	23						4.87 (Cubic)	0.49	4.06	0.10	9.8
NiFeAl	21	3.00	0.44	2.76	-0.04	93.8	2.48 (<i>Pnma</i>)	0.32	2.29	-0.03	55.5
NiFeGa	21	3.00	0.41	2.79	-0.08	100	2.64 (<i>P6₃/mmc</i>)	0.25	2.53	-0.05	60.5
NiFeSi	22	3.38	0.51	2.86	-0.01	76.8	1.72 (<i>Pnma</i>)	0.10	1.76	-0.04	71.2
NiFeGe	22	3.56	0.54	3.01	-0.01	72.4	2.37 (<i>P6₃/mmc</i>)	0.11	2.38	-0.05	59.8
NiFeP	23	3.64	0.57	2.94	0.05	76.7	1.08 (<i>P$\bar{6}2m$</i>)	0.18	0.96	-0.03	69.7
NiFeAs	23	3.71	0.56	3.03	0.04	78.8	2.08 (<i>P$\bar{6}2m$</i>)	-0.01	2.19	-0.03	57.2
NiFeS	24	<i>4.02</i>	<i>0.71</i>	<i>3.09</i>	<i>0.15</i>	97.2	2.00 (<i>Pnma</i>)	0.13	1.87	0.01	21.6

NiCrAs, NiFeS, PtCrP, PtMnSi, PtFeIn all in *Pnma* symmetry as well as PtMnIn in *P6₃/mmc* symmetry). Like a cubic case, there may be a possibility of half-metallicity in these non-cubic cases. A detailed analysis of DOS is warranted for the validation of the same (see next subsection). We analyze here the partial moments on the different atoms, present in the system. It is seen that in most of the cases the moments on the *B* and *C* atoms are anti-parallel to each other (Tables 5 to 7). However, the moments on the latter atoms are much smaller compared to the earlier ones as is observed in the cubic phase as well. Unlike the cubic case, no increasing trend in total moment as a function of *Z* of the *C* atom is observed for the lowest energy state. No trend is observed in the values of the total moments when the cubic and the *GS* states of any of the materials is compared. In majority of the cases the moments on the *B* and *A* atoms are found to be parallel to each other, including the Co-based compounds.

Spin Polarization at the Fermi Level – Next we discuss about the extent of spin polarization at the Fermi level (*SP*) of various materials in cubic versus the ground state. It is observed that except few of the *B=Fe* atom cases, *CoBC* materials possess high *SP* in the cubic case. For *NiBC*, only with the exception of NiMnSn and NiMnTe, all the cubic cases exhibit high *SP*. On the other hand, for *PtBC*, *SP* for the cubic cases seems to be below 50% for many of the alloys. Many, but not all, of the cubic structures of different materials exhibit a 100% *SP*. However, this is not the case with the lowest energy structure of any of the materials, which are studied in this paper. In the lowest energy case, we observe that only a few materials, with or without integral total moment, possess high *SP*, which is above 65%. While there are 6 of these, but none has a 100% *SP*. Out of these 6 cases, in ground state NiCrAs (*Pnma*) with a *SP* of 69.6 % and PtCrP (*Pnma*) with a *SP* of 66.4 % have a total integral moment of 2.99 and 3 μ_B , respectively. Further, for PtFeGe (*P $\bar{6}2m$*) has a moment of 1.99 and *SP* value of 71.9 %. However, while in the ground state, CoCrP (*Pnma*), NiFeSi (*Pnma*), NiFeP (*P $\bar{6}2m$*), and PtMnP (*P $\bar{6}2m$*) have comparable *SP* values of 76.3 %, 71.2 %, 69.7 % and 84.2 %, respectively, the corresponding total moments are 1.93, 1.72, 1.08 and 2.12 μ_B , respectively.

Table 7. Total and Partial Magnetic Moment per formula unit (in units of μ_B) for PtBC, calculated for cubic (*CS*) and the lowest energy structure (*GS*). NVE is the number of valence electrons, *SP* is the spin polarization at the Fermi level.

Material	NVE	<i>CS</i>					<i>GS</i>				
		μ_T	μ_A	μ_B	μ_C	<i>SP</i>	μ_T	μ_A	μ_B	μ_C	<i>SP</i>
PtCrAl	19	1.00	-0.07	1.17	-0.04	100	3.23 (<i>P6₃/mmc</i>)	0.09	3.04	-0.03	30.4
PtCrGa	19	1.00	-0.09	1.18	-0.06	100	3.28 (<i>P6₃/mmc</i>)	0.06	3.13	-0.05	36.8
PtCrIn	19	3.97	0.07	3.56	0.0	15.3	3.68 (<i>P6₃/mmc</i>)	0.06	3.46	-0.04	18.5
PtCrSi	20	2.00	-0.04	2.13	-0.07	100	3.08 (<i>Pnma</i>)	0.07	3.00	-0.08	6.5
PtCrGe	20	2.15	-0.19	2.43	-0.14	73.4	3.56 (<i>Pnma</i>)	0.06	3.42	-0.08	4.9
PtCrSn	20	3.24	-0.04	3.25	-0.09	20.9	3.61 (<i>Pnma</i>)	0.04	3.47	-0.07	42.7
PtCrP	21	3.00	-0.05	2.93	-0.08	100	3.00 (<i>Pnma</i>)	0.0	3.03	-0.09	66.4
PtCrAs	21	3.04	-0.09	3.04	-0.11	89.5	3.16 (<i>P$\bar{6}$2m</i>)	-0.08	3.26	-0.13	20.7
PtCrSb	21						3.19 (Cubic)	-0.07	3.24	-0.12	70.6
PtCrTe	22						4.01 (Cubic)	0.06	3.66	-0.06	95.5
PtMnAl	20	3.76	0.10	3.73	-0.05	70.7	3.51 (<i>P6₃/mmc</i>)	0.11	3.47	-0.04	39.2
PtMnGa	20	3.86	0.09	3.81	-0.07	61.8	3.79 (<i>P6₃/mmc</i>)	0.11	3.73	-0.06	35.3
PtMnIn	20	4.14	0.10	4.05	-0.05	53.5	4.01 (<i>P6₃/mmc</i>)	0.11	3.93	-0.05	18.5
PtMnSi	21	3.05	0.0	3.25	-0.09	25.4	3.05 (<i>Pnma</i>)	0.0	3.21	-0.06	14.9
PtMnGe	21	3.43	-0.11	3.70	-0.17	21.5	3.26 (<i>Pnma</i>)	-0.02	3.45	-0.10	0.99
PtMnSn	21						3.67 (Cubic)	0.02	3.82	-0.11	29.5
PtMnP	22	4.00	0.16	3.76	-0.04	100	2.12 (<i>P$\bar{6}$2m</i>)	0.04	2.16	-0.09	84.2
PtMnAs	22						4.01 (Cubic)	0.13	3.85	-0.08	76.5
PtMnSb	22						4.02 (Cubic)	0.11	3.93	-0.07	61.9
PtMnSe	23						4.74 (Cubic)	0.27	4.19	0.06	25.7
PtMnTe	23						4.83 (Cubic)	0.27	4.26	0.08	8.63
PtFeAl	21	3.00	0.19	2.99	-0.04	94.2	2.55 (<i>Pnma</i>)	0.12	2.55	-0.03	64.8
PtFeGa	21	3.00	0.17	3.01	-0.07	100	2.87 (<i>P6₃/mmc</i>)	0.11	2.88	-0.04	60.5
PtFeIn	21	3.00	0.14	3.10	-0.07	100	3.02 (<i>Pnma</i>)	0.11	3.02	-0.04	64.2
PtFeSi	22	3.30	0.27	3.03	-0.01	66.6	1.92 (<i>Pnma</i>)	0.02	2.07	-0.04	46.5
PtFeGe	22	3.94	0.38	3.47	0.01	38.4	1.99 (<i>P$\bar{6}$2m</i>)	0.05	2.06	-0.06	71.9
PtFeSn	22						3.53 (Cubic)	0.26	3.28	-0.01	77.6
PtFeP	23	3.73	0.39	3.16	0.06	45.4	1.18 (<i>P$\bar{6}$2m</i>)	0.05	1.24	-0.05	59.3
PtFeAs	23	3.69	0.35	3.21	0.04	62.3	1.27 (<i>P$\bar{6}$2m</i>)	0.0	0.99	-0.02	61.6
PtFeSb	23						3.57 (Cubic)	0.28	3.19	0.02	65.1

D. Analysis of Electronic Structure

Density of States of the Cubic Phase – For overall comparison of the trends, we plot in Figure 3, 4 and 5 the up and down DOS of the cubic and the lowest energy state of all the materials, including the ones with positive E_{form} . It is observed that the trends which are followed in case of the energetically stable ones are not strictly followed in case of the ones with positive E_{form} . The following trend is observed from Figure 3 for CoBC alloys. As the number of valence electrons of the *C* atom increases in a period, for example, Al to Si to P to S, the valence band width (VBW) is seen to increase systematically. Further, specifically for all the other cases, except a *C* atom from group VIA, the DOS shifts away from Fermi level, leading to a higher binding energy of the system. The DOS at and very close to Fermi level also changes. In case of S, Se and Te, these systematics are not consistently followed throughout. Furthermore, it is seen that when the *C* atom is from group IIIA, all the alloys of type CoBC are found to be energetically unstable. As the *Z* value of *C* atom increases in a group, for other groups, for example, Si to Ge to Sn, *i.e.* atoms with same NVE, not only the VBW, but also the DOS at the Fermi level remains similar. When the *A* atom changes, namely, Co atom is replaced by Ni and Pt, the shifting of the weight of the DOS curve towards lower energy (more binding energy) is clearly evident from Figures 4 and 5. The overall trends, near the Fermi level, as discussed above, are found to be the same. However, it is observed that while for *A*=Ni, most of the alloys are predicted to be energetically unstable, when the *A* atom is from group IIIA. For Pt all the alloys seem to have negative E_{form} and it is further to be noted that the weight of the DOS shifts towards lower energy making the systems more

bound in comparison to $A = \text{Co}$ or Ni , as is evident from the formation energies given in Tables 1 to 3 as well. As to why there is dip in the total moment (Figure 2), when the B atom is mainly an Mn atom and C atom is from group IVA, can be understood by analyzing the respective DOS curves. The up and down DOS in this case are seen to be more compensated leading to a lower moment when compared to the cases where C atoms are from other groups (Figures 3 to 5). As the Z value of B atom increases and the A and C atoms remain the same, the energy is lowered as Z of B atom increases, since the NVE of the system increases. However, it has been noted that, largely, the down spin DOS is more involved in all these, compared to the DOS of the up spin.

Comparison of DOS of Cubic versus Lowest Energy State – Figure 6, 7 and 8 give the total and partial DOS of the cubic and ground state of few materials. We have chosen different materials with various symmetries: while Figure 6 and 7 exhibit the DOS of $P6_3/mmc$ and $P6_2m$ symmetries, respectively, DOS of few materials for which $Pnma$ space-group is energetically the most favorable, is given in Figure 8. It is observed that as in these cases, and also in many other cases, there is a shift of weight of DOS of the ground state towards lower energy compared to the cubic state. Further, after critical analysis of DOS of ground versus the cubic state, the following few general points become note-worthy and relevant with regard to the non-cubic ground state symmetry of many materials (Tables 1 to 3). Mainly in the down spin DOS, a significant hybridization is noted between the A and C atoms, specifically, very close to the Fermi level.³³ A double-peak structure between the DOS of these two atoms is prominent in most of the cases. Further, hybridization between the B and C atoms and sometimes among all the three atoms is also observed. More than often this is found in the lower energy ranges (away from Fermi level) and also typically for up spin DOS. While cases with both Mn and Cr as B atoms show similar results, cases with Fe as B atom are slightly different: for example, the overlapping behavior with C and/or A atoms is better for up spin DOS and at lower energy compared to the vicinity of the Fermi level. These observations may explain the following: though, in the literature there is a lot of theoretical study on the cubic phases and half-metallicity in case of HHAs, experimentally many HHAs have been shown to prefer a lower symmetric structure and discussion about the HM-like behavior in a non-cubic case is generally missing from the literature.

DOS of Two Symmetries with Close E_{form} – Figure 9 gives the density of states for a few materials, for which two symmetries yield close to very close E_{form} and also geometry (Tables 1 to 4). As is evident from Table 3, for the material PtCrSn, two symmetries ($Pnma$ and $P6_3/mmc$) possess the same E_{form} within our calculational accuracy. The lowest panel in Figure 9 gives the support for the same from the electronic structure calculations. The total as well as partial DOS for this material in these two symmetries have an excellent matching. Similar is the case for PtMnIn and PtFeIn where the E_{form} values for these two phases are also very close.³³ Further, two materials PtMnSn and PtMnSb have a cubic phase as a lowest energy state. However, in the $GS+1$ (symmetry with higher energy than the ground state) and $GS+2$ (symmetry with higher energy than the $GS+1$ state) cases, PtMnSn has $P6_3/mmc$ and $Pnma$, respectively, while PtMnSb has $Pnma$ and $P6_3/mmc$, respectively. These two phases also have very similar formation energy. In Figure 9, we show the total and partial DOS for these $GS+1$ and $GS+2$ cases for PtMnSn and we observe that the DOS for these two cases are again matching very well. Similar is the case for PtMnSb.³³ As is evident from Tables 1 to 4 and Figure 9, the results of structural and electronic structure calculations are consistent for all these five materials mentioned here. On the contrary, when the E_{form} for one phase is slightly higher than the other (as in case of CeFeAs and NiMnAl), the peak positions and intensities of different peaks are not so alike as discussed above. Though in these two cases the E_{form} is different by only about 0.5 kJ/mol, from upper two panels it is seen that the matching of DOS of the two phases is not so excellent. The matching is slightly better in case of NiMnAl where the two symmetries involved are $P6_3/mmc$ and $Pnma$. This has been a general observation throughout. If $P6_3/mmc$ symmetry is found to be close to $Pnma$ symmetry, the matching of the geometry and electronic structure are very good. However, regarding the matching between $Pnma$ and $P6_2m$ symmetries, geometrical and electronic structures are seen to match only reasonably for these two phases even if energetically these phases are close to each other.³³ From literature on experimental studies of HHAs, it is observed that a very few cases exist where a material is reported to be in two different symmetries. Pertinent examples of such cases are NiMnAs, NiMnP, CoMnGe and NiMnGe. Figure 10 shows the DOS of the two experimentally reported phases for these materials. It is observed that both partial and total DOS are quite close for these two phases for all these materials. Since the difference between the two E_{form} values are more in case of CoMnGe, somewhat significant differences in total and partial DOS are visible from Figure 10.

DOS of Non-cubic HM-like States – Finally, we show the plot of density of states for a few materials which are likely to exhibit a HM-like behavior depending on the values of total (integral) moment in their non-cubic ground state. Figure 11 exhibits the DOS of CoMnP, CoFeP, NiCrAs and PtCrP which show a gap or a pseudo-gap with a very low DOS at the Fermi level, for one of the spin channels, for both the ground state and the cubic phase. The cases of NiCrAs and PtCrP in the lowest energy state ($Pnma$ phase) are reasonably clear. A very small density of states at the Fermi level is observed for the down spin channel of both the materials. However, the DOS at the up spin channel is also somewhat small for both the cases. This results in an effective spin polarization (at the Fermi level) of about 70 and 66% for NiCrAs and PtCrP in the ground state, respectively. Contrary to these cases, both CoMnP

and CoFeP will probably behave as a bad semi-metal rather than a half-metal since there are small densities of states at both the spin channels, up DOS being slightly larger in intensity than the down DOS. We note from Tables 5 to 7 that, these four materials possess total moments which are very close to integers. Total moment of 3, 2, 2 and $3 \mu_B$ are observed for CoMnP, CoFeP, NiCrAs and PtCrP, respectively. There are few other materials, for which also, in the non-cubic case, the total moment is very close to an integer. These cases include NiFeS, PtMnSi, PtFeIn - having the $Pnma$ (See Tables 5 to 7), and also PtMnIn - having the $P6_3/mmc$ space-group, respectively. In these cases also, our calculations reveal the appearance of a pseudo-gap at the down spin channel.³³ However, the DOS at the Fermi level for the up spin channel, though is higher compared to the DOS for the down spin electron, the absolute value of the DOS for down spin electron is not negligible, as is observed in the case of NiCrAs and PtCrP. Further, we consider the cases of some other materials with high SP but with total moment not so close to an integer value. It has been observed that out of these materials, in the ground state, CoCrP and NiFeSi have $Pnma$, and NiFeP and PtMnP have $P\bar{6}2m$ symmetries; and as discussed above, these have total moment of 1.93, 1.72, 1.08 and $2.12 \mu_B$, respectively. The corresponding SP has been observed to be high and comparable to those of NiCrAs and PtCrP. Therefore, we observe that, though there is no rigorous one-to-one relationship among the cubic symmetry, integral total moment and high SP , but a strictly half-metallic behavior (with exactly 100% SP) and integral total moment are found to be associated only with the cubic symmetry. Hence, by combined analysis of magnetic and electronic structure calculations, CoCrP, NiCrAs, NiFeSi, NiFeP, PtCrP and PtMnP alloys are predicted to be non-cubic half Heusler alloys with significantly high SP . However, the point to be noted here is that a high SP does not necessarily indicate a possibility of semiconducting behavior along one spin channel, and in turn, a possible application of a material as an appropriate spin-injector material. Hence we predict from our present density of states calculations that NiCrAs and PtCrP are the only two non-cubic materials which in their $Pnma$ phase may have a potential in this regard and also these are magnetic in nature. This observation awaits the experimental validation.

IV. CONCLUSION

In this paper geometric, electronic, and magnetic properties of Ni, Co and Pt-based half Heusler alloys, namely, $NiBC$, $CoBC$ and $PtBC$ ($B = Cr, Mn$ and Fe ; $C = Al, Si, P, S, Ga, Ge, As, Se, In, Sn, Sb$ and Te) have been calculated in detail using first principles calculations based on density functional theory. Quite a few of these materials with a C atom from group IIIA, IVA and VA have already been experimentally and/or theoretically found in various different symmetries. In this work, we probe the stability of all the above-mentioned alloys in different crystal symmetries, reported in the literature. These structures include, the most common (face-centered) cubic $C1_b$ phase (space-group $F\bar{4}3m$), and also orthorhombic (space-group $Pnma$), as well as hexagonal (space-groups $P\bar{6}2m$ and $P6_3/mmc$) phases. We find from our calculations of formation energy that along with alloys with C elements from group IIIA, IVA and VA, alloys with C elements from group VIA are also, by and large, energetically stable. It has also been observed that high Z elements as the C atom lead to stabilized phases in case of the Pt-based compounds. On the contrary, it is not so in the case of Co and Ni-based materials.

In literature half-metallicity in many half and full Heusler alloys have been shown to exist which is typically associated with a cubic symmetry. We note from the results of the magnetic properties calculations, that there is a possibility of existence of some novel non-cubic half-metallic-like half Heusler alloys, as these possess total integer moments. Therefore, to discuss the relative stabilities of different symmetries in order to search for the respective lowest energy state for all the materials as well as to ascertain whether a material is half-metallic or not, we analyze the partial and total density of states. Based on the results of the magnetic and electronic properties, (i) we show that for a material depending on the hybridization between different atoms a particular symmetry is more stable compared to the cubic or other phases; (ii) we observe that there is no rigorous *one-to-one relationship* between the *cubic symmetry* and *high spin polarization at the Fermi level*; (iii) it is found that a strictly half-metallic behavior (with 100% spin polarization) is associated only with the cubic symmetry; (iv) along with a few new cubic half-metallic alloys, we predict the possibility of existence of a few novel *non-cubic* alloys with significantly low DOS in one of the spin channels and *high spin polarization at the Fermi level*.

V. ACKNOWLEDGEMENT

Authors thank P. A. Naik, T. Ganguli and Arup Banerjee for facilities and constant encouragement throughout the work. The scientific computing group of computer centre, RRCAT, Indore and P. Thander are thanked for help in

installing and support in running the codes.

-
- ¹ I. Zutic, J. Fabian, S. Das Sharma, *Rev. Mod. Phys.* **76**, 323 (2004); S.A. Wolf, D.D. Awschalom, R.A. Buhrman, J.M. Daughton, S. von Molnar, M.L. Roukes, A.Y. Chtchelkanova, D.M. Treger, *Science*, **294**, 1488 (2001).
 - ² R.A.de Groot, F.M. Mueller, P.G. van Engen, K.H.J. Buschow, *Phys. Rev.Lett.*, **50**, 2024 (1983); R.A. de Groot, K.H.J.Buschow, *J. Magn. and Magn. Mater.*, **5457**, 1377 (1986) ; I. Galanakis, P. H. Dederichs and N. Papanikolaou *PHys. Rev. B* **66**, 134428 (2002).
 - ³ J. Ma, V. I. Hegde, K. Munira, Y. Xie, S. Keshavarz, D. T. Mildebrath, C. Wolverton, A. W. Ghosh, W. H. Butler, *Phys. Rev. B*, **95**, 024411 (2017) and the references therein.
 - ⁴ Tufan Roy, Dhanshree Pandey, Aparna Chakrabarti, *Phys. Rev. B*, **93**, 184102 (2016) and references therein.
 - ⁵ Tufan Roy, Aparna Chakrabarti, *J. Magn. Magn. Mater.*, **423**, 396 (2017).
 - ⁶ P. G. van Engen, K. H. J. Buschow, R. Jongebreur, M. Erman, *Appl. Phys. Lett.*, **42**, 202 (1983); P. J. Webster, K. R. A. Ziebeck, *Alloys and Compounds of d-elements with Main Group Elements*, Springer, Berlin, Germany, **75** (1988); K. R. A. Ziebeck, K. U. Neumann, *Magnetic Properties of Metals*, Springer, Berlin, Germany, **64** (2001); H.C. Kandpal, G.H. Fecher, C. Felser, *J. Phys. D: Appl. Phys.*, **40**, 1507 (2007); H. Zenasni, H.I. Faraoun, C. Esling, *J. Magn. Magn. Mater.*, **333**, 162 (2013); V. Sharma, A.K. Solanki, A. Kashyap, *J. Magn. Magn. Mater.* **322**, 2922 (2010); H.Z. Luo, F.B. Meng, Z.Q. Feng, Y.X. Li, W. Zhu, G.H. Wu, X.X. Zhu, C.B. Jiang, H.B. Xu, *J. Appl. Phys.*, **105**, 103903 (2009); J. Bai, J.M. Raulot, Y.D. Zhang, C. Esling, X. Zhao, L. Zuo, *J. Appl. Phys.*, **109** 014908 (2011); N. Xu, J.M. Raulot, Z.B. Li, J. Bai, Y.D. Zhang, X. Zhao, L. Zuo, C. Esling, *Appl. Phys. Lett.*, **100**, 084106 (2012); F. Casper, T. Graf, S. Chadov, B. Balke, C. Felser, *Semicond. Sci. and Tech.*, **27**, 063001 (2012); J. Chen, G.Y. Gao, K.L. Yao, M.H. Song, *J. Alloys and Comp.*, **509**, 10172 (2011).
 - ⁷ T. Block, M. J. Carey, B. A. Gurney, O. Jespen, *Phys. Rev. B*, **70**, 205114 (2004); S. Gardelis, J. Androulakis, P. Miggiakis, J. Giapintzakis, S. K. Clowes, Y. Bugoslavsky, W. R. Branford, Y. Miyoshi, L. F. Cohen, *J. Appl. Phys.*, **95**, 8063 (2004); S. K. Ren, J. Gao, X. L. Jiang, G. B. Ji, W. Q. Zou, F. M. Zhang, Y. W. Du, *J. Alloy Comp.*, **384**, 22 (2004); S. K. Ren, W. Q. Zou, J. Gao, X. L. Jiang, F. M. Zhang, Y. W. Du, *J. Magn. Magn. Mater.*, **288**, 276 (2005); Z. Wen, T. Kubota, T. Yamamoto, K. Takanashi, *Sci. Rep.*, **5**, 18387 (2015).
 - ⁸ E. L. Habbak, R. Shabara, S. H. Aly and S. Yehia, *Physica B : Cond. Mater.*, **494**, 63 (2016); V. A. Dinh, K. Sato and H. K. Yoshida, *IEEE Trans. Magnetism*, **45**, 2663 (2009); S. Y. Lin, X. B. Yang, Y. J. Zhao, *J. Magn. Magn. Mater.*, **350**, 119 (2014); Y. Wu, B. Wu, Z. Wei, Z. Zhou, C. Zhao, Y. Xiong, S. Tou, S. Yang, B. Zhou, Y. Shao, *Intermetallics*, **53**, 26 (2014); M.P. Ghimire, Sandeep, T.P. Sinha, R.K. Thapa, *J. Alloys and Comp.*, **509**, 9742 (2011); L. Offernes, P. Ravindran, A. Kjekshus, *J. Alloys and Comp.* **439**, 37 (2007); M. Zhang, X. Dai, H. Hu, G. Liu, Y. Cui, Z. Liu, J. Chen, J. Wang and G. Wu, *J. Phys. : Cond. Mater.* **15**, 7891 (2003); E. Sasioglu, L. M. Sandratskii, and P. Bruno, *J. Appl. Phys.* **98**, 063523 (2005); I. Galanakis, K. Ozdogan, and E. Sasioglu, *J. Appl. Phys.*, **104**, 083916 (2008); V. A. Dinh, K. Sato, and H. K. Yoshida, *J. Phys. Soc. Jpn.*, **77**, 014705 (2008); R. A. de Groot, K. H. J. Buschow, *J. Magn. Magn. Mater.*, **54-57**, 1377 (1986); P. P. J. van Engelen, D. B. de Mooij, J. H. Wijngaard, K. H. J. Buschow, *J. Magn. Magn. Mater.*, **130**, 247 (1994); J. F. Bobo, P. R. Johnson, M. Kautzky, F. B. Mancoff, E. Tuncel, R. L. White, B. M. Clemens, *J. Appl. Phys.*, **81**, 4164 (1997); V. A. Dinh, K. Sato, and H. K. Yoshida, *J. Comput. Theor. Nanosci.*, **6**, 2589 (2009); M. Singh, H. S. Saini, S. Kumar, M. K. Kashyap, *Comput. Mater. Sci.*, **53**, 431 (2012); L. Feng, E. K. Liu, W. X. Zhang, W. H. Wang, G. H. Wu, *J. Magn. Magn. Mater.*, **351**, 92 (2014); Z. Yao, Y. S. Zhang, and K. L. Yao, *Appl. Phys. Lett.*, **101**, 062402 (2012).
 - ⁹ M. J. Otto, H. Feil, R. A. M. van Woerden, J. Wijngaard, P. J. V. Andervalk, C. F. van Bruggen, A. Haas, *J. Magn. Magn. Mater.*, **70**, 33 (1987) and the references therein.
 - ¹⁰ G. A. Landrum, R. Hoffmann, J. Evers and H. Boysen, *Inorg. Chem.*, **37**, 5754 (1998).
 - ¹¹ M. R. Montreuil, B. Deyris and A. Michel, *Mat. Res. Bull.*, **7**, 813 (1972).
 - ¹² M. A. Nylund, M. A. Roger, J. P. Senateur and R. Fruchart, *J. Solid Stat. Chem.*, **4**, 115 (1972),
 - ¹³ J. Wirringa, R. Wartchow and M. Binnewies, *Kristallogr. NCS*, **215**, 197 (2000).
 - ¹⁴ S. Niziol, A. Bombik, W. Baielal, A. Szytula and D. Fruchart, *J. Magn. Magn. Mater.*, **27**, 281 (1982).
 - ¹⁵ A. Szytula, A.T. Pedziwiatr, Z. Tomkowicz and W. Bazela, *J. Magn. Magn. Matter.* **25**, 176 (1981).
 - ¹⁶ R. Fruchart, A. Roger, and J. P. Senateur, *J. Appl. Phys.* **40**, 1250 (1969).
 - ¹⁷ V. Johnshon, *Mat. Res. Bull.*, **8**, 1067 (1973).
 - ¹⁸ J. P. Senateur, A. Rouault and R. Fruchart and D. Fruchart, *J. Solid Stat. Chem.*, **5**, 226 (1972).
 - ¹⁹ T. Kanomata, H. Endo, H. Yamauchi, Y. Yamaguchi, H. Yoshida, T. Kaneko, H. Aruga Katori, T. Goto, *Physica B*, **237-238**, 517 (1997).
 - ²⁰ Y. Ma, S. Yang, Y. Zhou, C. Wang and X. Liu, *Intermetallics*, **18**, 2105 (2010).
 - ²¹ H. Fjellvag and A.F. Andresen, *J. Magn. Magn. Mater.* **50**, 291 (1985).
 - ²² H. M. V. Noort, D. B. de Mooij and K. H. J. Buschow, *Phys. Status Solidi A*, **86**, 655 (1984).
 - ²³ K.H.J. Buschow, J. H. N. van Vucht, P.G. van Engen, D. B. de Mooij and A. M. van der Kraan, *Phys. Stat. Solidi A*, **75**, 617 (1983).
 - ²⁴ K.H.J. Buschow, P.G. van Engen, R. Jongebreur, *J. Magn. Magn. Mater.*, **38**, 1 (1983).
 - ²⁵ S. Niziol, A. Bombik, W. Bazela, A. Szytula and D. Fruchart, *J. Magn. Magn. Mater.* **27** 281 (1982).
 - ²⁶ M. J. Otto, H. Feil, R. A. M. Van Woerden, J. Wijngaard, P. J. Van Der Valk, C. F. Van Bruggen, C. Haas, *J. Magn. Magn.*

- Mater., **70**, 33 (1987).
- ²⁷ V. Ksenofontov, G. Melnyk, M. Wojcik, S. Wurmehl, K. Kroth, S. Reiman, P. Blaha, C. Felser, Phys. Rev. B, **74**, 134426 (2006).
- ²⁸ K. H. J. Buschow and D. B. de Mooij, Journal of the Less-Common Metals, **99**, 125 (1984).
- ²⁹ Y. Ma, S. Yang, Y. Zhou, C. Wang, X. Liu, Intermetallics, **18**, 2105 (2010).
- ³⁰ G. Kresse, J. Furthmüller, Phys. Rev. B, **54**, 11169 (1996); G. Kresse, D. Joubert, Phys. Rev. B, **59**, 1758 (1999); VASP 5.2 program package is fully integrated in the MedeA platform (Materials Design, Inc.) with a graphical user interface enabling the computation of the properties.
- ³¹ P. E. Blochl, Phys. Rev. B, **50**, 17953 (1994).
- ³² J. P. Perdew, K. Burke, M. Ernzerhof, Phys. Rev. Lett., **77**, 3865 (1996).
- ³³ Madhusmita Baral et. al. (manuscript in preparation).
- ³⁴ P. Blaha, K. Schwartz, G. K. H. Madsen, D. Kvasnicka and J. Luitz, WIEN2K, An Augmented Plane Wave plus Local Orbitals Program for Calculating Crystal Properties, (Karlheinz Schwarz, Tech. Universität, Wien, Austria), 2002, ISBN 3-9501031-1-2.
- ³⁵ J. E. Saal, S. Kirklin, M. Aykol, B. Meredig, C. Wolverton, JOM, **65**, 1501 (2013); S. Kirklin, J. E. Saal, B. Meredig, A. Thompson, J. W. Doak, M. Aykol, S. Rühl, C. Wolverton, NPJ Comput. Mater., **1**, 15010 (2015).
- ³⁶ W. H. Butler, A. W. Ghosh, *et. al.*, "Heuslers home", <http://heusleralloys.mint.ua.edu/> (2016).
- ³⁷ H. C. Kandpal, G. H. Fecher, C. Felser, J. Phys. D: Appl. Phys., **40**, 1507 (2007).
- ³⁸ I. Galanakis, P. H. Dederichs, N. Papanikolaou, Phys. Rev. B, **66**, 174429 (2002).

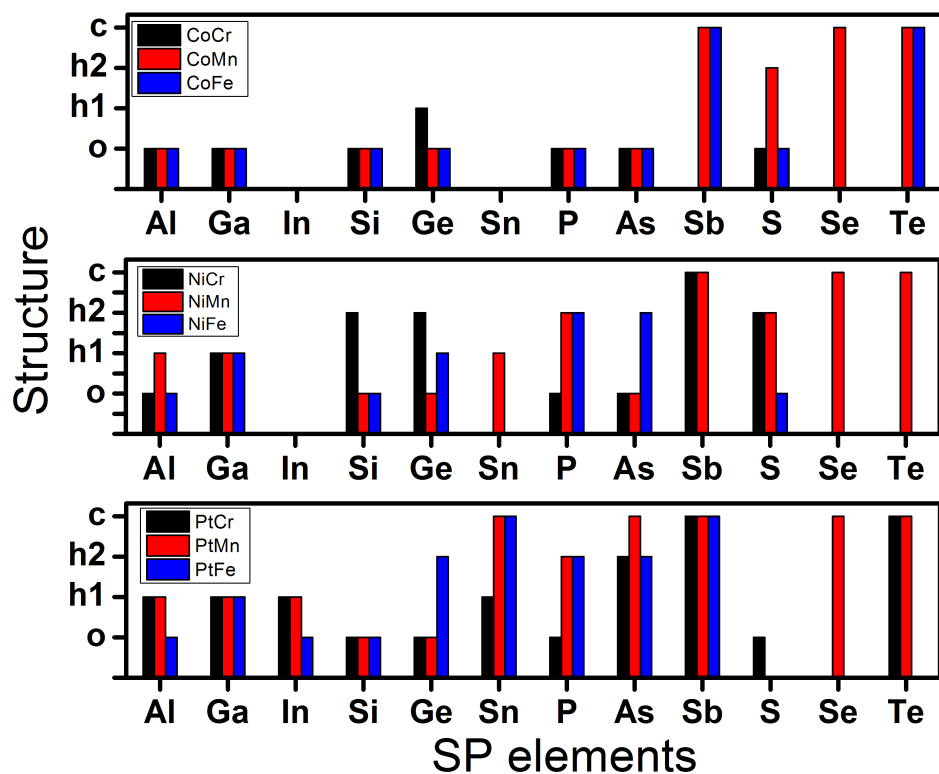


FIG. 1: The optimized symmetry for each of the 83 energetically stable compounds, which is obtained on the basis of formation energy. *o*, *h1*, *h2* and *c* signify $Pnma$, $P6_3/mmc$, $P\bar{6}2m$ and $F\bar{4}3m$ space-groups, respectively.

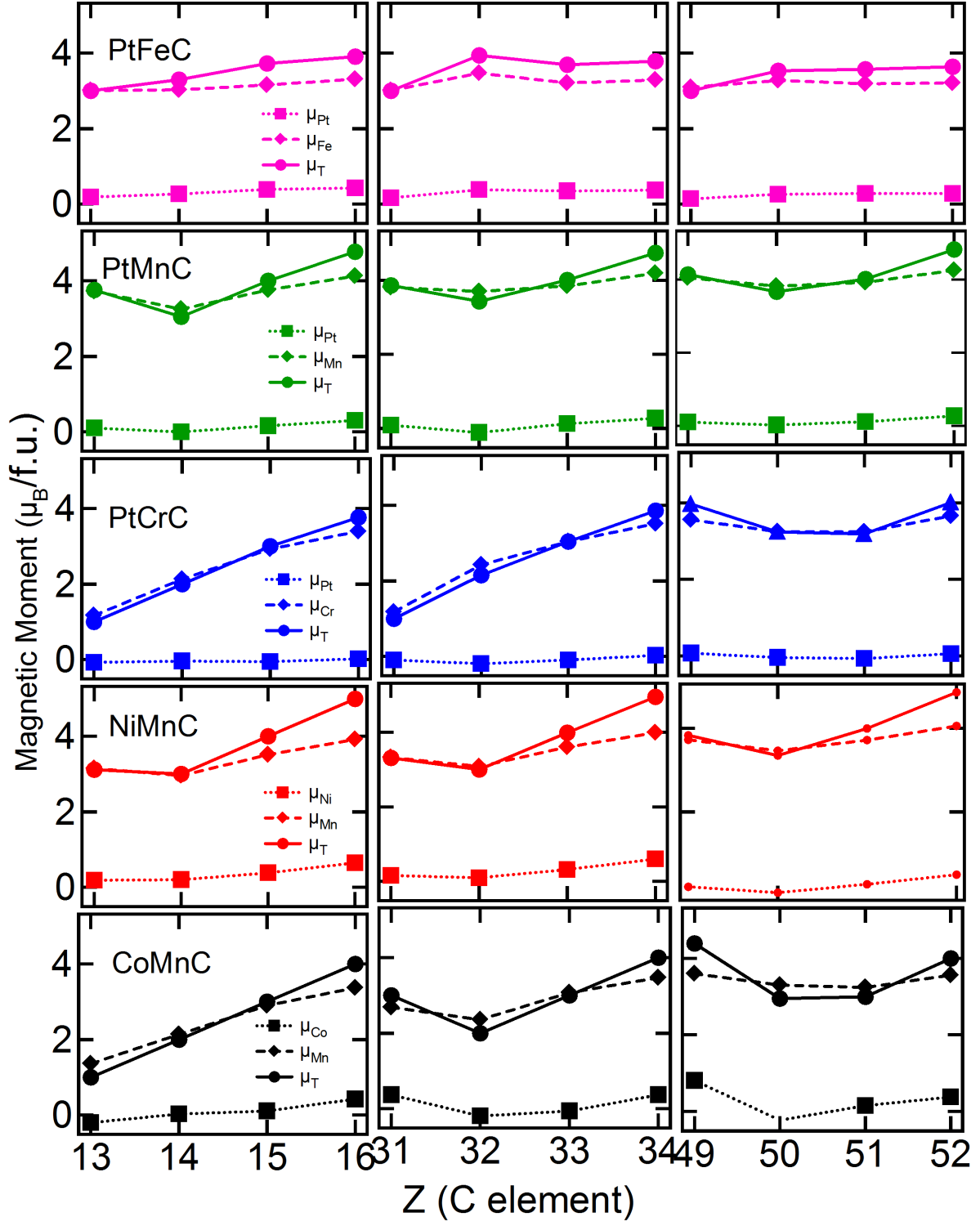


FIG. 2: The total and partial moments of some of the $CoBC$, $NiBC$ and $PtBC$ alloys as a function of atomic number of C atoms.

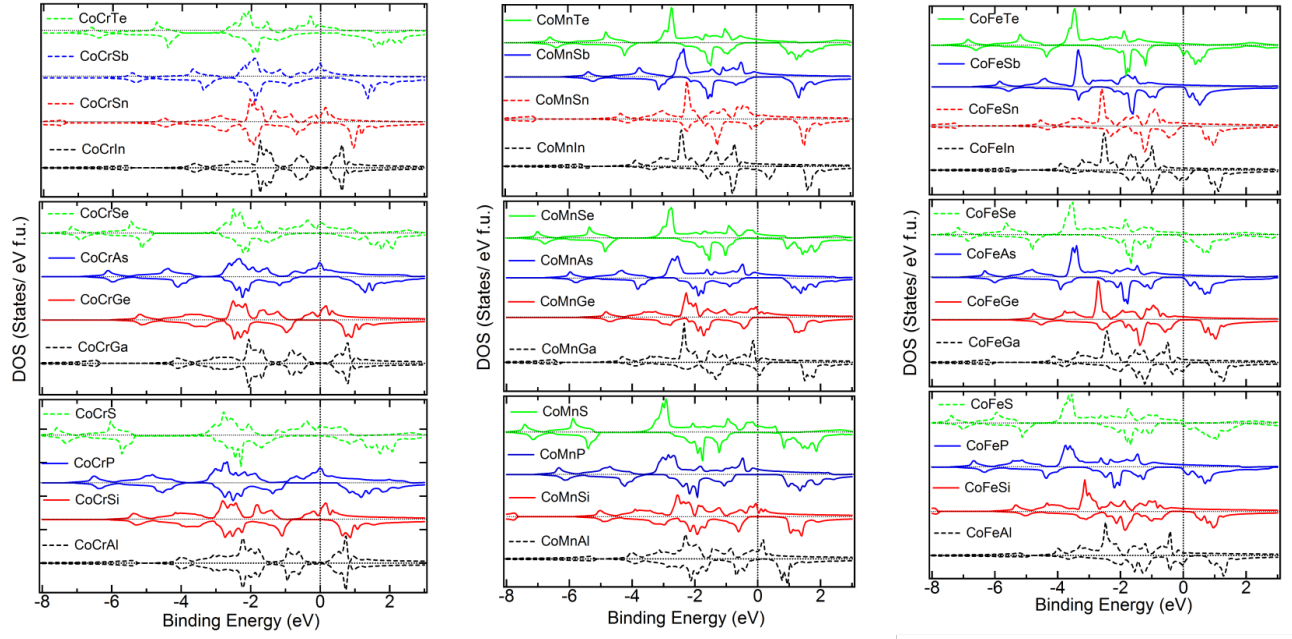


FIG. 3: The up and down total density of states of CoBC alloys in the cubic phase. The DOS of stable alloys in terms of formation energy are plotted with a solid line and DOS of energetically unstable alloys are plotted with a dotted line.

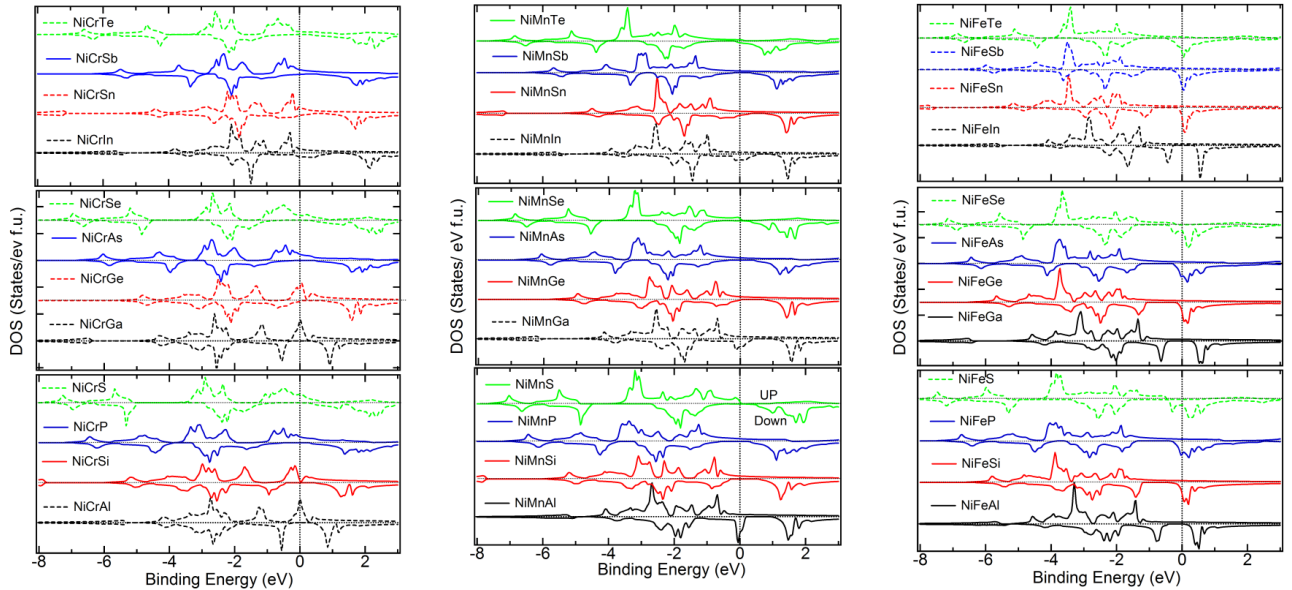


FIG. 4: The up and down density of states of NiBC alloys in the cubic phase. The DOS of stable alloys in terms of formation energy are plotted with a solid (red) line and DOS of energetically unstable alloys are plotted with a (black) dotted line.

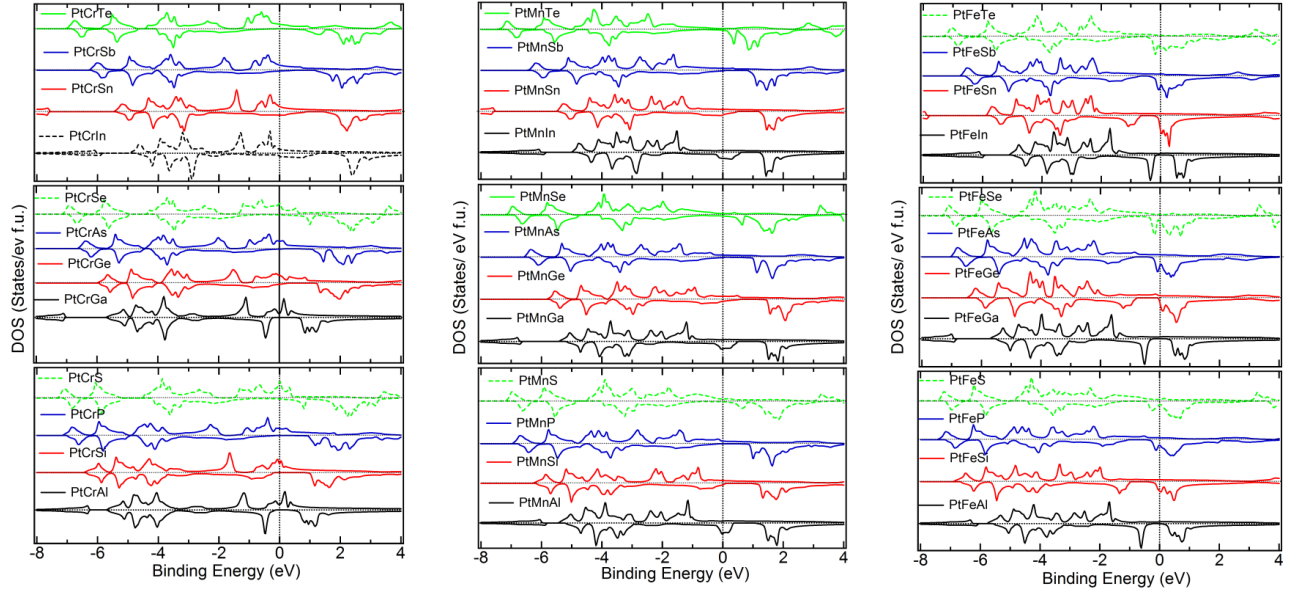


FIG. 5: The up and down density of states of PtBC alloys in the cubic phase. The DOS of stable alloys in terms of formation energy are plotted with a solid (red) line and DOS of energetically unstable alloys are plotted with a (black) dotted line.

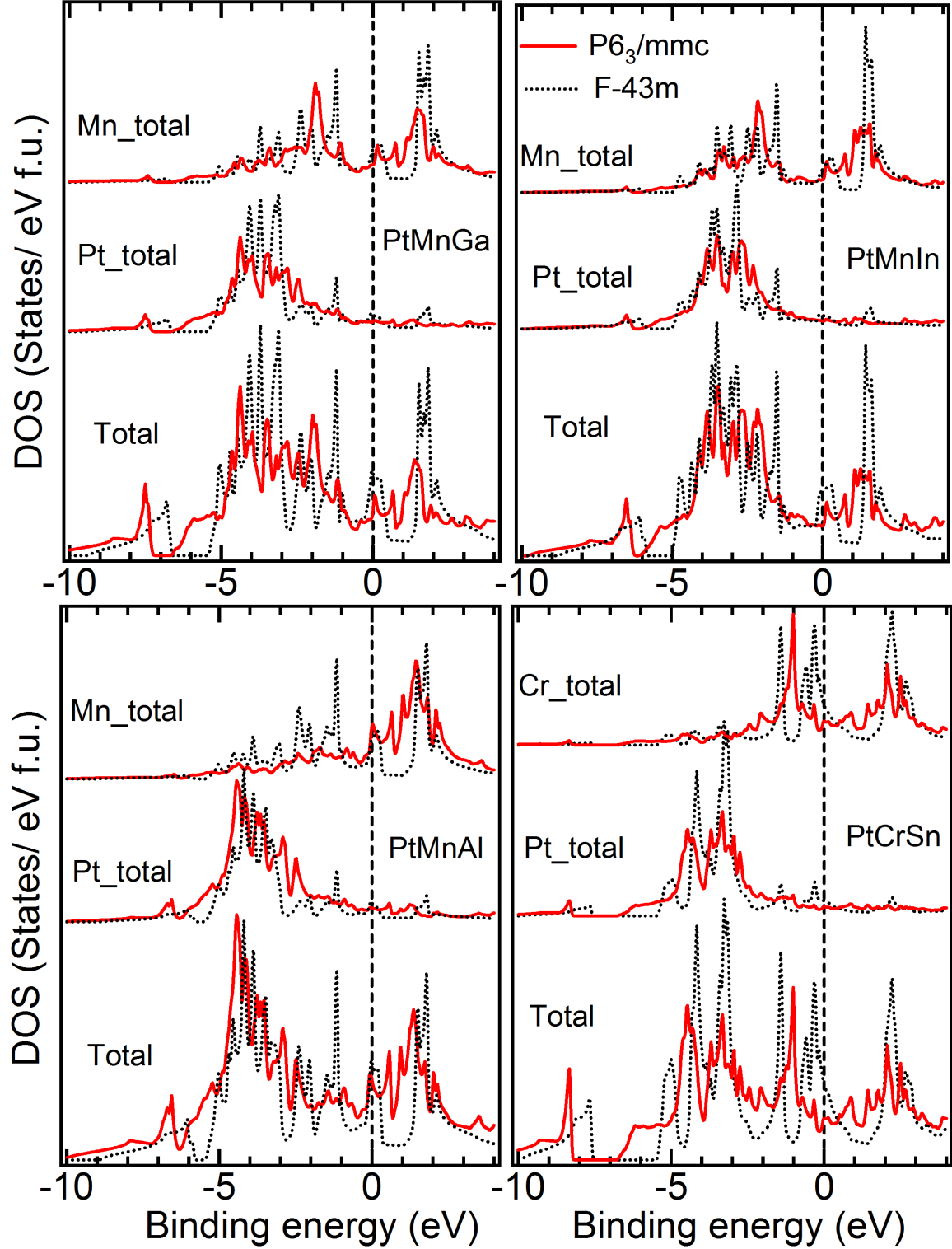


FIG. 6: The total and partial DOS of the cubic and ground state of a few materials with $P6_3/mmc$ symmetry. The DOS of ground state is plotted with a solid (red) line and DOS of cubic phase is plotted with a (black) dotted line.

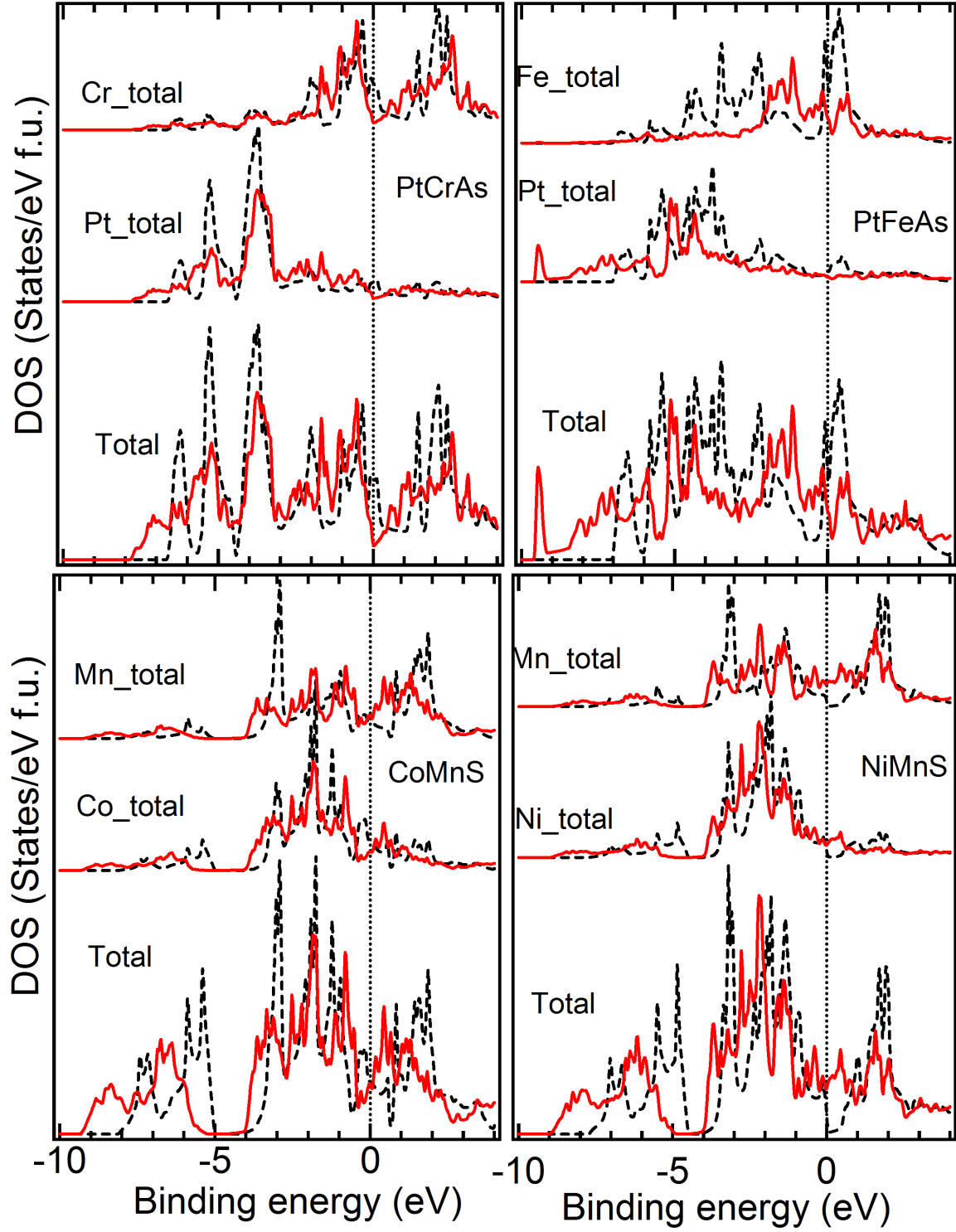


FIG. 7: The total and partial DOS of the cubic and ground state of a few materials with $P\bar{6}2m$ symmetry. The DOS of ground state is plotted with a solid (red) line and DOS of cubic phase is plotted with a (black) dotted line.

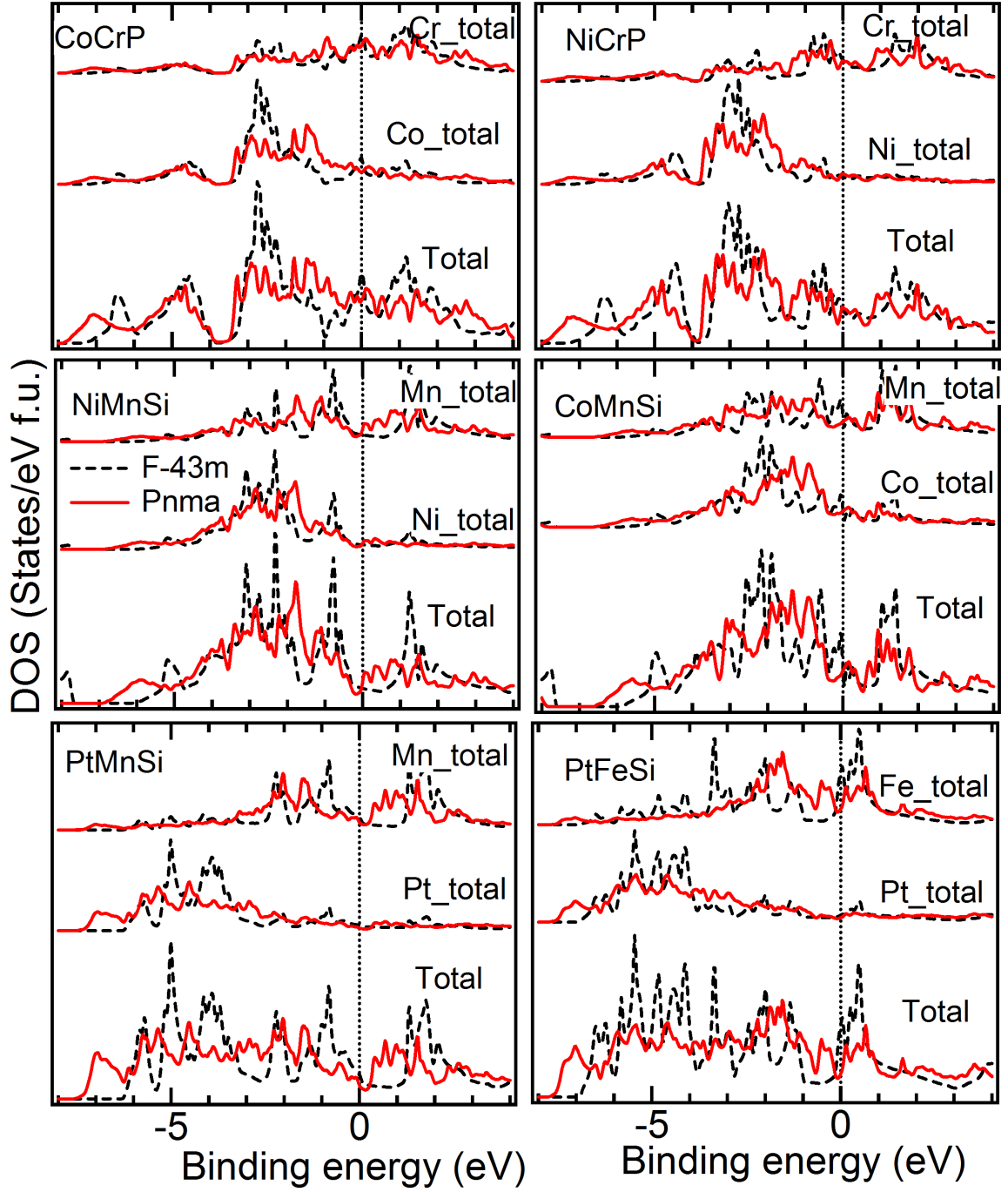


FIG. 8: The total and partial DOS of the cubic and ground state of a few materials with $Pnma$ symmetries. The DOS of ground state is plotted with a solid (red) line and DOS of cubic phase is plotted with a (black) dotted line.

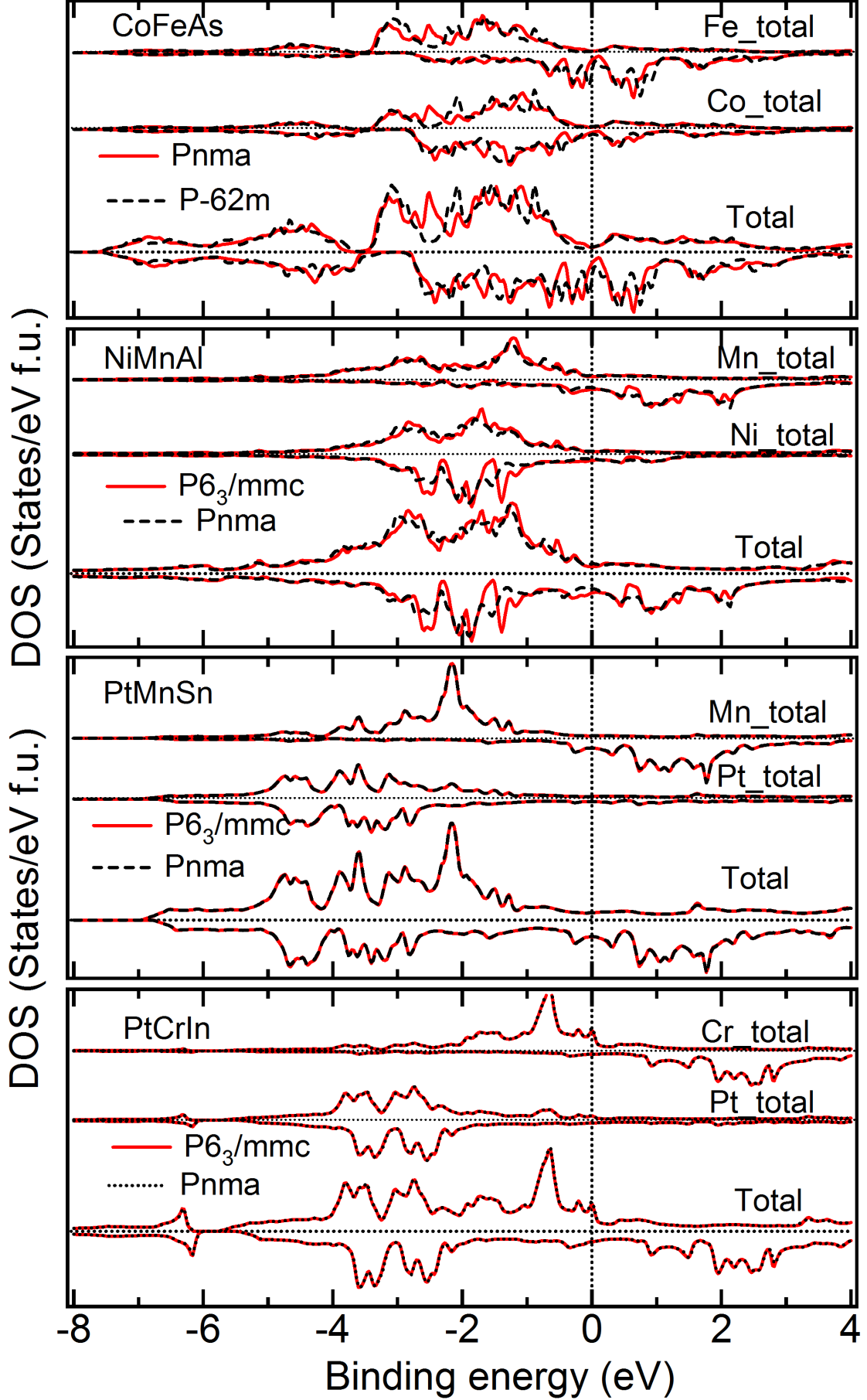
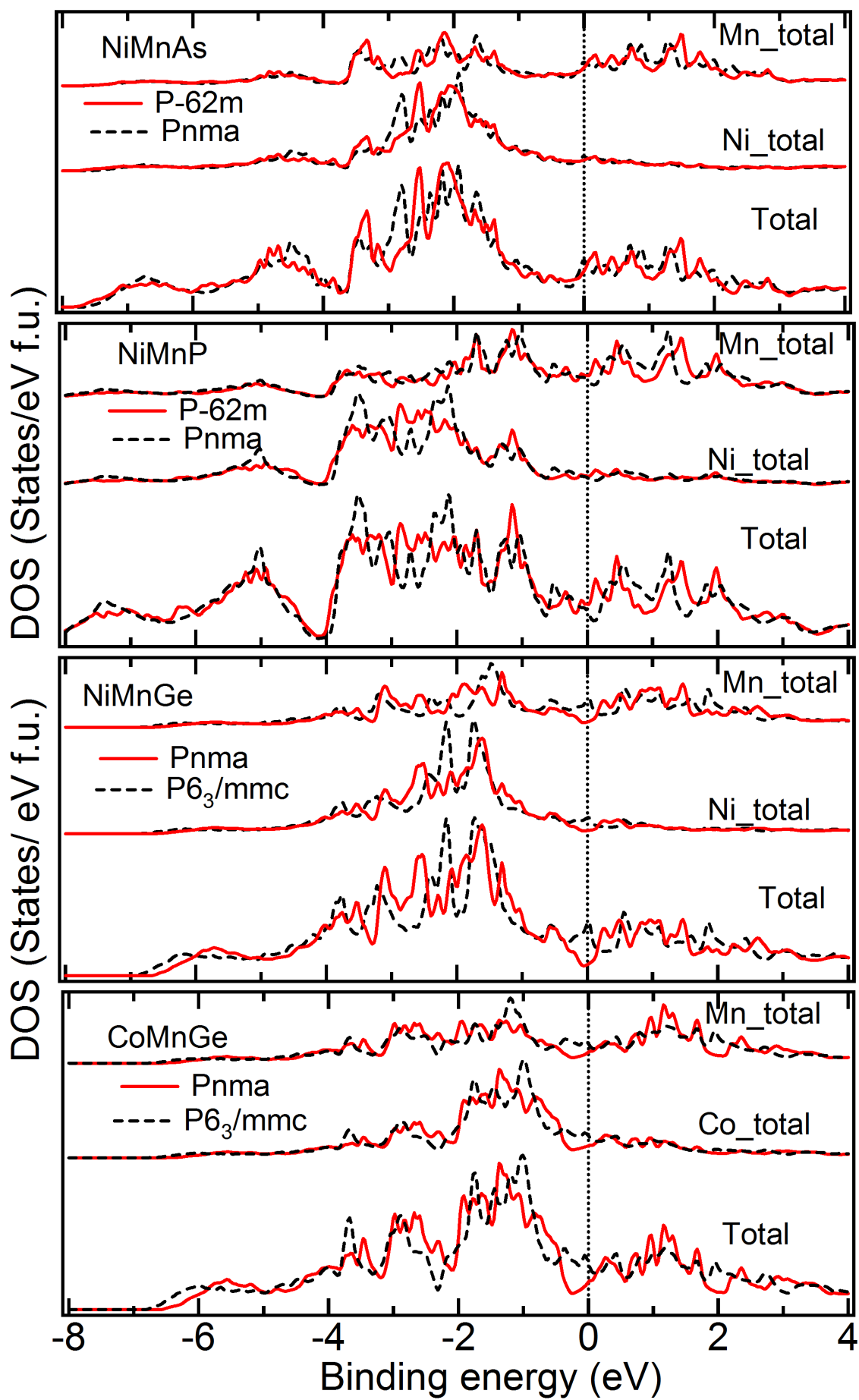


FIG. 9: The total density of states and DOS of *A* and *B* atoms, for a few materials, for which two symmetries yield close



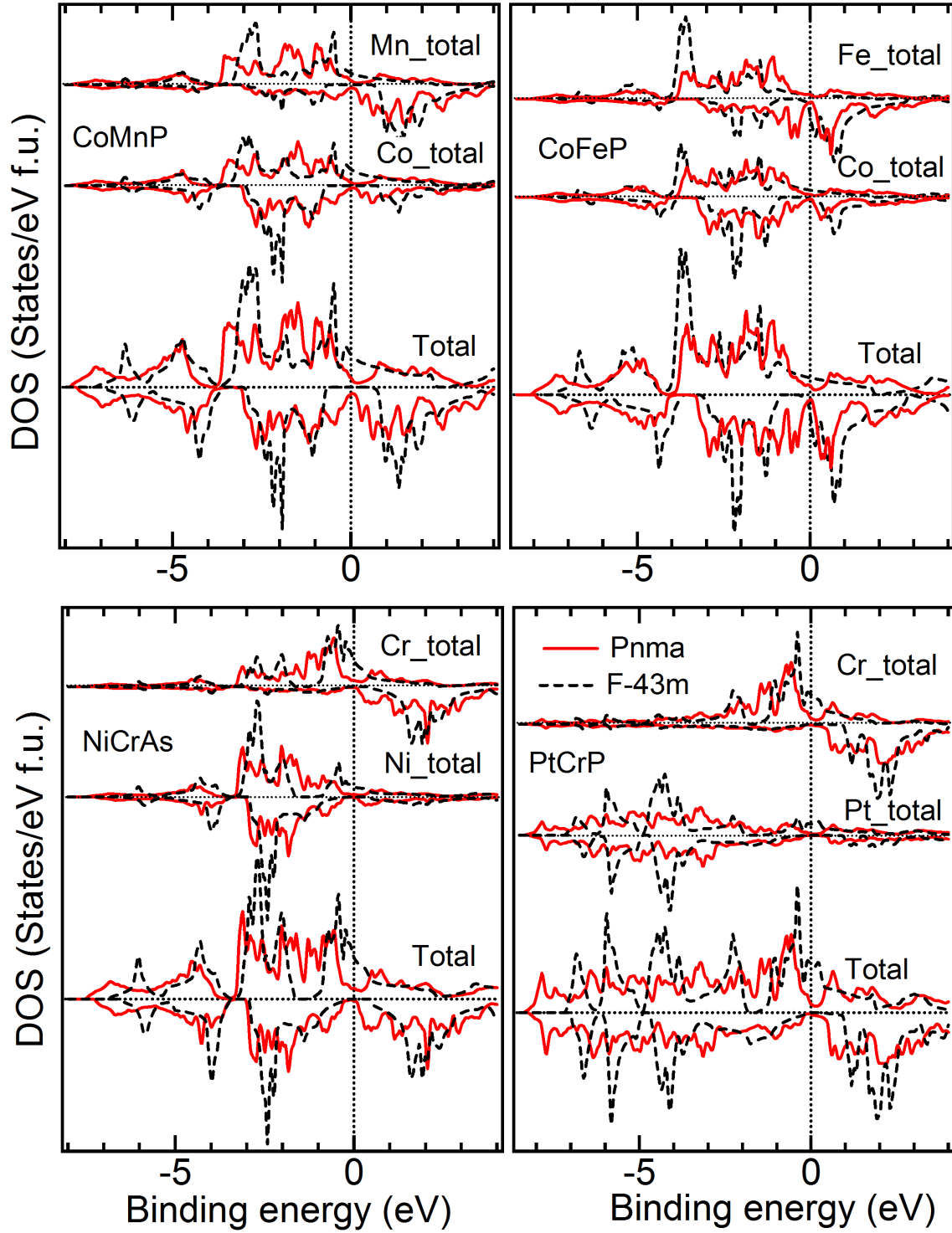


FIG. 11: The total density of states and DOS of A and B atoms, for a few materials, for the non-cubic ground state and cubic phases: in lower panels DOS of CoMnP and CoFeP and in upper panels, DOS NiCrAs and PtCrP are shown. The DOS of one phase is plotted with a solid (red) line and DOS of the other phase is plotted with a (black) dotted line.